

SCIENTIFIC REPORTS



OPEN

Extremely Low Frequency Electromagnetic Fields Facilitate Vesicle Endocytosis by Increasing Presynaptic Calcium Channel Expression at a Central Synapse

Received: 27 September 2015

Accepted: 01 February 2016

Published: 18 February 2016

Zhi-cheng Sun^{1,*}, Jian-long Ge^{1,*}, Bin Guo^{2,*}, Jun Guo¹, Mei Hao¹, Yi-chen Wu¹, Yi-an Lin¹, Ting La¹, Pan-tong Yao¹, Yan-ai Mei³, Yi Feng⁴ & Lei Xue¹

Accumulating evidence suggests significant biological effects caused by extremely low frequency electromagnetic fields (ELF-EMF). Although exo-endocytosis plays crucial physical and biological roles in neuronal communication, studies on how ELF-EMF regulates this process are scarce. By directly measuring calcium currents and membrane capacitance at a large mammalian central nervous synapse, the calyx of Held, we report for the first time that ELF-EMF critically affects synaptic transmission and plasticity. Exposure to ELF-EMF for 8 to 10 days dramatically increases the calcium influx upon stimulation and facilitates all forms of vesicle endocytosis, including slow and rapid endocytosis, endocytosis overshoot and bulk endocytosis, but does not affect the RRP size and exocytosis. Exposure to ELF-EMF also potentiates PTP, a form of short-term plasticity, increasing its peak amplitude without impacting its time course. We further investigated the underlying mechanisms and found that calcium channel expression, including the P/Q, N, and R subtypes, at the presynaptic nerve terminal was enhanced, accounting for the increased calcium influx upon stimulation. Thus, we conclude that exposure to ELF-EMF facilitates vesicle endocytosis and synaptic plasticity in a calcium-dependent manner by increasing calcium channel expression at the nerve terminal.

During the past few decades, considerable evidence has shown that non-thermal exposure to extremely low frequency electromagnetic fields (ELF-EMF)¹ can induce biological changes both *in vivo* and *in vitro*, including gene expression², tissue repair, and proliferation³, and it can also be conducive to the treatment of neurological disorders^{4,5}. Despite accumulating experimental evidence suggesting significant biological effects, the underlying mechanisms are poorly understood. Laboratory studies have pointed to the initial effects of ELF-EMF being on the cellular level, especially the physiological properties of the cell membrane and channels^{6–10}. Therefore, the neurons in the central nervous system are likely to be the most sensitive candidates, as exposure to ELF-EMF induces electrical fields and currents, which may excite or suppress neuronal activities through interactions with voltage-gated channels^{11,12}.

Vesicle endocytosis, which couples to exocytosis and recycles exocytosed vesicles at the presynaptic nerve terminal, is a basic cellular mechanism that critically maintains synaptic transmission and plasticity^{13–15}. Membrane fission caused by endocytosis also contributes to the homeostasis of the plasma membrane^{14,16}. Although endocytosis fulfils such a crucial role in both physical and physiological aspects, very few studies regarding how ELF-EMF regulates this important cellular event in the central nervous system were reported and data from

¹State Key Laboratory of Medical Neurobiology, Department of Physiology and Biophysics, School of Life Sciences and Collaborative Innovation Centre for Brain Science, Fudan University, Shanghai, 200438, P.R.China. ²Institute of Genetics, State Key Laboratory of Genetic Engineering, Fudan University, Shanghai, 200433, P.R.China. ³Institutes of Brain Science, School of Life Sciences and State Key Laboratory of Medical Neurobiology, Fudan University, Shanghai, 200438, P.R.China. ⁴Department of Critical Care Medicine, Shanghai General Hospital, Shanghai Jiaotong University, Shanghai, 200080, P.R.China. *These authors contribute equally to this work. Correspondence and requests for materials should be addressed to Y.F. (email: orchidfy@hotmail.com) or L.X. (email: lxue@fudan.edu.cn)

experimental studies are controversial¹⁷. In the present study, we directly measured vesicle exocytosis and endocytosis with accurate capacitance measurements^{14,18} at a central synapse, the calyx of Held. At calyces, several forms of endocytosis have been reported, including slow endocytosis¹⁴, rapid endocytosis¹⁹, endocytosis overshoot²⁰, and bulk endocytosis²¹, and their underlying molecular mechanisms are different. Slow endocytosis is believed to be clathrin-dependent, whereas the others are not²². Whether exposure to ELF-EMF affects all forms of endocytosis is unknown.

Calcium, a mediator of intracellular signalling, has also been proposed to be affected by magnetic fields. In U937 cells, magnetic fields increase calcium influx and inhibit apoptosis²³. In rat pituitary cells, exposure to 50 Hz magnetic fields increases the intracellular free calcium concentration²⁴. However, this facilitation of intracellular calcium could not be independently replicated^{25–27}. In addition, no effect on calcium influx was observed in isolated bovine chromaffin cells exposed to ELF-EMF up to 2.0 milliTesla (mT)²⁸. In our study, we performed direct presynaptic measurements of calcium influx at calyces and suggested an increased calcium influx using different stimulation protocols. The post-tetanic potentiation (PTP), a calcium-dependent form of short-term plasticity, was also facilitated by the increased calcium influx after exposure to ELF-EMF. It is well accepted that calcium influx triggers exocytosis at nerve terminals, and we previously showed that calcium/calmodulin initiates all forms of endocytosis^{14,18,19}, suggesting that the increased calcium influx accounts for the regulation of endocytosis after exposure to ELF-EMF. Thus, the voltage-gated calcium channels at the presynaptic nerve terminals may be the key factor underlying such ELF-EMF modulation¹¹.

In this study, we provide for the first time direct evidence that ELF-EMF facilitates all forms of endocytosis and potentiates PTP^{16,29}. Furthermore, the enhanced expression of calcium channels at the presynaptic nerve terminal, especially the P/Q type, increases calcium influx upon stimulation and facilitates vesicle endocytosis and synaptic plasticity. Our study provides novel insight into how ELF-EMF regulates neuronal activity and plasticity by increasing voltage-dependent calcium channels at the cellular level.

Materials and Methods

Electromagnetic field production. The system used to generate a magnetic field was similar as previously described³⁰. Briefly, a 50 Hz magnetic field was generated by a pair of Helmholtz coils powered by a generator system producing the input pulse. The magnetic flux densities were adjusted to 1 mT and monitored by an electromagnetic field sensor with a digital multi-meter. The whole system could provide a uniform electromagnetic field for the animals within it.

Slice preparation and electrophysiology. Postnatal day 8–10 (p8 – p10) old C57 mice of either sex were used in this study. The ELF-EMF exposure group was raised in the electromagnetic field from the day of birth (p0). Brain slice preparation was similar as previously reported^{14,15,19}. Briefly, pups were decapitated and blocks of tissue containing the medial nucleus of the trapezoid body (MNTB) were placed in artificial cerebrospinal fluid (ACSF) solution (in mM: 125 NaCl, 25 NaHCO₃, 3 myo-inositol, 2 Na-pyruvate, 2.5 KCl, 1.25 NaH₂PO₄, 0.4 ascorbic acid, 25 glucose, 3 MgCl₂, and 0.05 CaCl₂). Brain slices ~200 μm thick were prepared using a vibratome (VT 1200 s, Leica, Germany) and recovered in 37 °C with 95% O₂ and 5% CO₂ for 30 minutes before experiments. Electrophysiological recordings were made at room temperature (22–24 °C). Whole-cell capacitance measurements were made using the EPC-10 amplifier (HEKA, Lambrecht, Germany) with software lock-in amplifier. The presynaptic pipette (3.5–5 MΩ) solution contained (in mM): 125 Cs-gluconate, 20 CsCl, 4 Mg-ATP, 10 Na₂-phosphocreatine, 0.3 GTP, 10 HEPES, and 0.05 BAPTA (pH 7.2, adjusted with CsOH). The series resistance (<10 MΩ) was compensated by 65% (lag 10 μs). For recordings of the PTP, a bipolar electrode was placed at the midline of the trapezoid body. A 0.1 ms, 2–20 V voltage pulse was applied to evoke an action potential, which induced an AMPA receptor-mediated excitatory postsynaptic current (EPSC) at the postsynaptic principal neuron. 1 mM kynurenic acid (KYN) was added to the bath solution to relieve AMPA receptor saturation and desensitization^{19,31}. Voltage-clamp recordings of EPSCs and mEPSCs were made with an EPC 10 amplifier using pipettes (2–3 MΩ) containing (in mM): 125 K-gluconate, 20 KCl, 4 Mg-ATP, 10 Na₂-phosphocreatine, 0.3 GTP, 10 HEPES, and 0.5 EGTA (pH 7.2, adjusted with KOH). The series resistance (<10 MΩ) was compensated by 90% (lag 10 μs). Statistical analysis used a t test unless otherwise noted, and means were presented as mean ± SE. All the methods were carried out in accordance with the approved guidelines and all animal experimental protocols were approved by the Animal Care and Use Committee of Fudan University.

Western blot. Membrane proteins of calyces were extracted from both control and ELF-EMF exposure groups using Membrane and Cytosol Protein Extraction Kit (with membrane protein extraction reagent B, Beyotime Biotechnology, China) as described in previous study³². Protein samples were resolved on 10% SDS-PAGE and then transferred to PVDF membrane in transfer buffer (25 mM Tris, 192 mM glycine, and 20% methanol) for 20 min at 15 V. The membrane was blocked in TBS-T (20 mM Tris-HCl adjusted to pH 7.4, 500 mM NaCl, and 0.1% Tween 20) containing 5% non-fat milk at room temperature for 30 min and then probed with specific antibody overnight at 4 °C (pan and P/Q types: Abcam, USA; N type: Alomone, USA; R type: Sigma, USA). The membrane was blotted with horseradish peroxidase (HRP)-conjugated secondary antibody (Jackson, diluted 1:5000 in TBS-T with 5% non-fat milk) at room temperature for 30 min. After a final wash in TBS-T, the signal was detected using the ChemiDoc MP System (Bio-rad) according to the manufacturer's instructions.

Real-time PCR. Total RNA was extracted from calyces with TRIzol reagent (Invitrogen, USA). The concentration of RNA was measured using a NanoDrop 2000 spectrophotometer (Thermo Fisher, USA) with an OD₂₆₀/OD₂₈₀ ratio of 2.0. About 200 ng of total RNA was reverse-transcribed into cDNA using TransScript One-Step gDNA Removal and cDNA Synthesis SuperMix Kit (TransGen Biotech, China). All RNA and cDNA samples were stored at –70 °C before use.

Primer name	Sequence (5' - 3')
GAPDH-F	AGGTCGGTGTGAACGGATTTG
GAPDH-R	TGTAGACCATGTAGTTGAGGTCA
P/Q-F	CTCAACTCCACCCTGATGGC
P/Q-R	AATGGCCATCATCTCCTTGCG
N-F	GTACCACCCACAAAACCTGAC
N-R	CAGAGGGTGGAAACAGGAAAC
R-F	ACTCTCATGTACCACCGCTA
R-R	GTGTGGAGGTGAAGTGGACTG

Table 1. Primer sequences for real-time PCR.

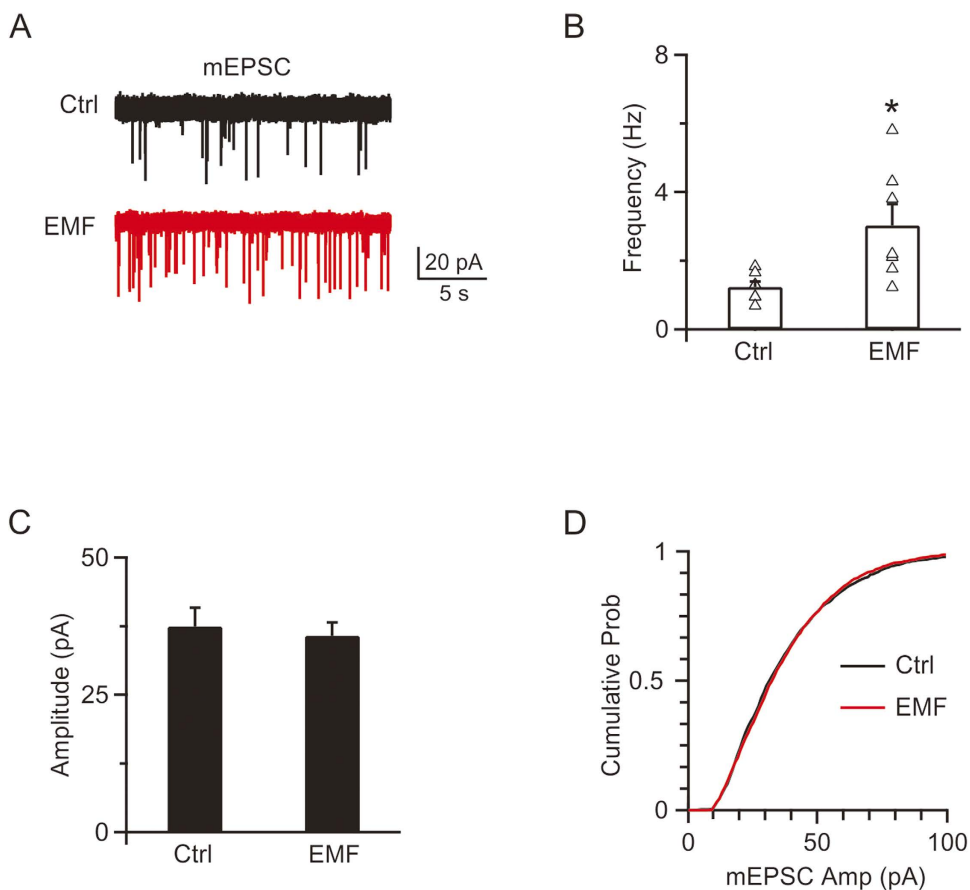


Figure 1. ELF-EMF exposure increases mEPSC frequency (A) Upper: sampled mEPSC in controls. Lower: sampled mEPSC in the ELF-EMF exposure group. (B) Mean of the mEPSC frequency distributions plotted for individual cells in the control and ELF-EMF exposure groups (triangle). (C) Mean of the mEPSC amplitude in the control (1363 events from 7 cells) and ELF-EMF exposure groups (1758 events from 7 cells). (D) The cumulative probability distribution in the control (black) and ELF-EMF exposure groups (red).

Gene expression of all three calcium channel subtypes (P/Q, N, and R) was quantified by real-time PCR using SYBR® Premix DimerEraser™ (Takara, Japan). The glyceraldehyde-3-phosphate dehydrogenase (GAPDH) gene was used as an internal control to normalise expression level of calcium channel genes. The primer sequences used are shown in Table 1.

Results

ELF-EMF increases mEPSC frequency but does not affect mEPSC amplitude. To evaluate how ELF-EMF regulates synaptic transmission, C57 mice were raised in a 50 Hz, 1 mT electromagnetic field from birth. Pups of p8–p10 from the control and ELF-EMF exposure groups were used to record mEPSCs. Whole cell voltage clamp recordings of mEPSCs are shown in Fig. 1A. In controls, the averaged mEPSC frequency and amplitude were 1.2 ± 0.2 Hz and 37.5 ± 3.4 pA, respectively (1363 events from 7 cells, Fig. 1B,C). However, exposure to ELF-EMF significantly increased the mEPSC frequency to 3.0 ± 0.6 Hz ($n = 7$, $p < 0.05$), though it did not

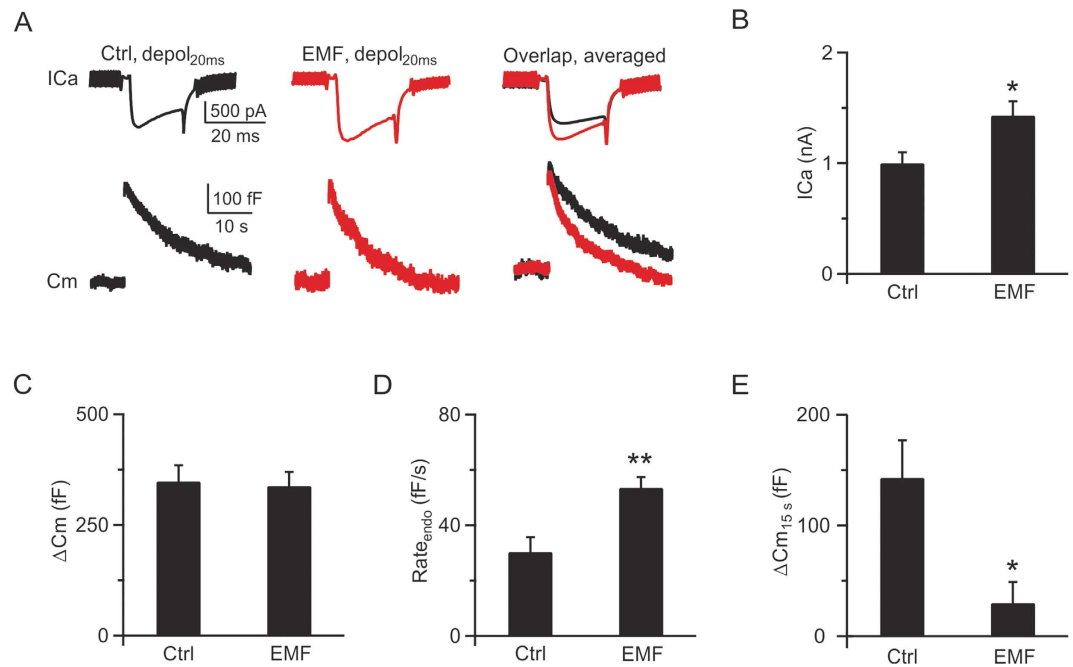


Figure 2. ELF-EMF exposure accelerates slow endocytosis (A) Left: Sampled presynaptic calcium current (ICa, upper) and membrane capacitance (Cm, lower) induced by a 20 ms depolarisation (depol_{20ms}) in controls. Middle: Similar to Left, but for the ELF-EMF exposure group. Right: The averaged ICa (upper) and Cm (lower) from the control (n = 5, black) and ELF-EMF exposure groups (n = 5, red). (B–E) Statistics for ICa, ΔCm, Rate_{endo}, and ΔCm_{15s} in the control and ELF-EMF exposure groups (*p < 0.05; **p < 0.01).

affect the mEPSC amplitude (36.0 ± 2.4 pA, 1758 events from 7 cells; $p = 0.7$, Fig. 1B,C). The cumulative plots also confirmed that the amplitude distribution was not significantly different ($p = 0.6$, K-S test, Fig. 1D). The frequency increase in the ELF-EMF exposure group suggested a potential presynaptic mechanism^{16,29}. However, the increase in presynaptic vesicle release frequency also raised the question of how neurons could maintain synaptic transmission with limitedly available vesicles at nerve terminals^{15,22,33}.

ELF-EMF facilitates both slow and rapid endocytosis. To further explore how ELF-EMF affects synaptic transmission, we examined synaptic vesicle exocytosis and endocytosis at presynaptic nerve terminals. We previously showed that different stimulation protocols induce different kinetics of exo-endocytosis^{14,18}. A 20 ms depolarisation pulse (depol_{20ms}, depolarised from -80 mV to $+10$ mV, same as below if not mentioned) can deplete the readily releasable pool (RRP) and induce a following clathrin-dependent, dynamin-dependent slow endocytosis^{13,14,34}, whereas 10 depolarisation pulses of 20 ms at 10 Hz (depol_{20msx10}) can induce a larger amount of exocytosis and an additional rapid form of endocytosis that depends on dynamin but not clathrin^{18,19,34,35}. In p8–p10 pups exposed to ELF-EMF, the depol_{20ms} induced a mean calcium influx of 1.4 ± 0.1 nA (n = 5; Fig. 2A, middle), which was larger than that in controls (1.0 ± 0.1 nA, n = 5, $p < 0.05$; Fig. 2A, left, 2B). The increased calcium influx did not significantly affect exocytosis (control: 348 ± 36 fF, n = 5; ELF-EMF: 338 ± 32 fF, n = 5; $p = 0.8$; Fig. 2A, right) because depol_{20ms} was strong enough to deplete the whole RRP, which was similar in both groups (Fig. 2C, see Supplementary Information II for detailed discussion on how EMF affects exocytosis and vesicle release probability). However, depol_{20ms} resulted in a significant difference in endocytosis after exposure to ELF-EMF. The mean endocytosis rate (Rate_{endo}) was 54 ± 4 fF/s (n = 5) in the ELF-EMF exposure group, which was much faster than that in controls (30 ± 5 fF/s, n = 5, $p < 0.01$; Fig. 2D). The net capacitance increase 15 s after the stimulation (ΔCm_{15s}) was 31 ± 20 fF (Fig. 2E) in the ELF-EMF exposure group, reflecting an almost full recovery. However, the ΔCm_{15s} in controls was larger (144 ± 28 fF, $p < 0.05$; Fig. 2E), further confirming the acceleration of slow endocytosis after ELF-EMF exposure.

Next, we investigated whether ELF-EMF also affected the rapid form of endocytosis induced by intense stimulation^{18,19}. In controls, depol_{20msx10} evoked a calcium influx (QICa) of 187 ± 16 pC (Fig. 3A, left, 3B) and a total capacitance jump (ΔCm) of 1057 ± 42 fF (n = 5, Fig. 3C), which was followed by a bi-exponential capacitance decay with time constants of 2.0 ± 0.1 s (amplitude, 250 ± 37 fF) and 18.0 ± 5.2 s, respectively (Fig. 3A, left and right). The initial endocytosis rate (Rate_{endo}) measured within 2 s after depol_{20msx10} was 114 ± 13 fF/s, which reflects the speed of membrane retrieval caused by rapid endocytosis (Fig. 3D)^{14,18}. In the ELF-EMF exposure group (Fig. 3A, middle), depol_{20msx10} evoked a larger calcium influx of 230 ± 8 pC (n = 6, $p < 0.05$; Fig. 3B) with a similar amount of exocytosis (1105 ± 103 fF, n = 6, $p = 0.7$; Fig. 3A, right, 3C). However, the endocytosis rate accelerated dramatically after depol_{20msx10}. The capacitance decay could fit well with time constants of 1.1 ± 0.4 s (n = 6; amplitude, 364 ± 60 fF) and 14.0 ± 3.3 s, respectively (Fig. 3A, middle and right). The Rate_{endo} also increased to 193 ± 23 fF/s (n = 6, $p < 0.01$; Fig. 3D). Taken together, the increased Rate_{endo} decreased time

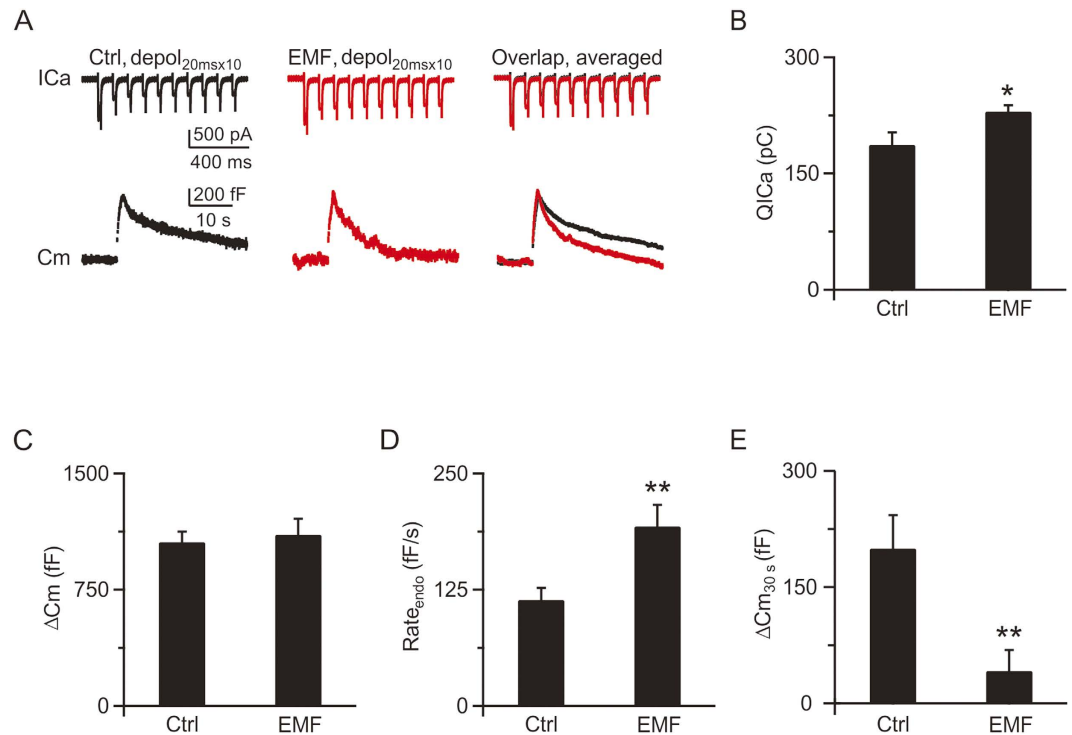


Figure 3. ELF-EMF exposure accelerates rapid endocytosis (A) Left: Sampled presynaptic calcium current (ICa, upper) and membrane capacitance (Cm, lower) induced by $\text{depol}_{20\text{ms} \times 10}$ in controls. Middle: Similar to Left, but for the ELF-EMF exposure group. Right: The averaged ICa (upper) and Cm (lower) from the control (n = 5, black) and ELF-EMF exposure groups (n = 6, red). (B–E) Statistics for QICa, ΔC_m , Rate_{endo} and ΔC_m_{30s} in the control and ELF-EMF exposure groups (*p < 0.05; **p < 0.01).

constant (τ_{rapid}), and increased size of the rapid component of endocytosis clearly indicated an acceleration of rapid endocytosis¹⁸. Furthermore, the increase in net capacitance 30 s after stimulation in the ELF-EMF exposure group was much smaller than in the control group (control: 200 ± 42 fF, ELF-EMF: 41 ± 27 fF, p < 0.01; Fig. 3E), which also confirmed the acceleration of endocytosis.

ELF-EMF facilitates endocytosis overshoot and bulk endocytosis. Endocytosis overshoot, which retrieves more membrane than immediate exocytosis, has been reported in secretory cells and nerve terminals (Fig. 4A)^{20,36}. We previously showed that the chance of observing endocytosis overshoot increases as calcium influx increases, from ~50% with 2 mM extracellular calcium to ~70% when calcium increases to 5.5 mM after 10 depolarisation pulses of 50 ms at 10 Hz ($\text{depol}_{50\text{ms} \times 10}$) in rats²⁰. Having shown that exposure to ELF-EMF increases the calcium influx during $\text{depol}_{20\text{ms}}$ or $\text{depol}_{20\text{ms} \times 10}$ stimulation, we investigated whether ELF-EMF also increases the fraction of calyces demonstrating endocytosis overshoot. In 7 out of 31 control calyces (23%), we observed significant endocytosis overshoot (>250 fF) after $\text{depol}_{50\text{ms} \times 10}$ (5.5 mM calcium in bath) with a mean size of 709 ± 96 fF (Fig. 4B,C). This proportion is much smaller than previously reported in rats (~70%)²⁰ because the calcium influx during $\text{depol}_{50\text{ms} \times 10}$ was also much smaller than in rats. For example, the calcium influx induced by the first 50 ms depolarisation during $\text{depol}_{50\text{ms} \times 10}$ was only 92 ± 9 pC (n = 7) in mice but approximately 150 pC in rats²⁰. Although the mean amplitude of endocytosis overshoot (709 ± 96 fF, n = 7) was smaller than in rats (~1000 fF), it was still roughly twice the RRP size in mice (348 fF from Fig. 2C), which was similar as reported in rats. In the ELF-EMF exposure group, the number of calyces demonstrating endocytosis overshoot dramatically increased (Fig. 4C, chi-square test, p < 0.05). In 15 out of 30 mice, we observed significant endocytosis overshoot with a mean size of 631 ± 80 fF (n = 15, p = 0.6; Fig. 4B,C). The increased proportion of calyces demonstrating endocytosis overshoot in the ELF-EMF exposure group was consistent with the larger calcium influx compared to controls (measured from the first 50 ms depolarisation during $\text{depol}_{50\text{ms} \times 10}$, control: 92 ± 9 pC, n = 7; ELF-EMF group: 119 ± 10 pC, n = 15; p < 0.01). However, the mean endocytosis overshoot size was not significantly different between the two groups, suggesting the same source from stranded vesicles at the presynaptic terminal in both groups^{18,20,34}.

Bulk endocytosis, which directly retrieves a large piece of membrane from the presynaptic plasma membrane, has also been reported in neuronal cells (Fig. 4D)^{18,21,37}. We previously reported that the frequency of bulk endocytosis increases with more intense stimulation, and buffering intracellular calcium with 70 mM EGTA abolishes bulk endocytosis¹⁸. Since ELF-EMF could increase the calcium influx, we further investigated whether it can also regulate bulk endocytosis. In 6 out of 32 control calyces, we observed obvious bulk endocytosis after $\text{depol}_{50\text{ms} \times 10}$ (5.5 mM calcium in bath) with a mean size of 159 ± 36 fF (measured by the downward capacitance step, DCS; Fig. 4E,F). In 8 out of 26 calyces in the ELF-EMF exposure group, we observed obvious bulk endocytosis with

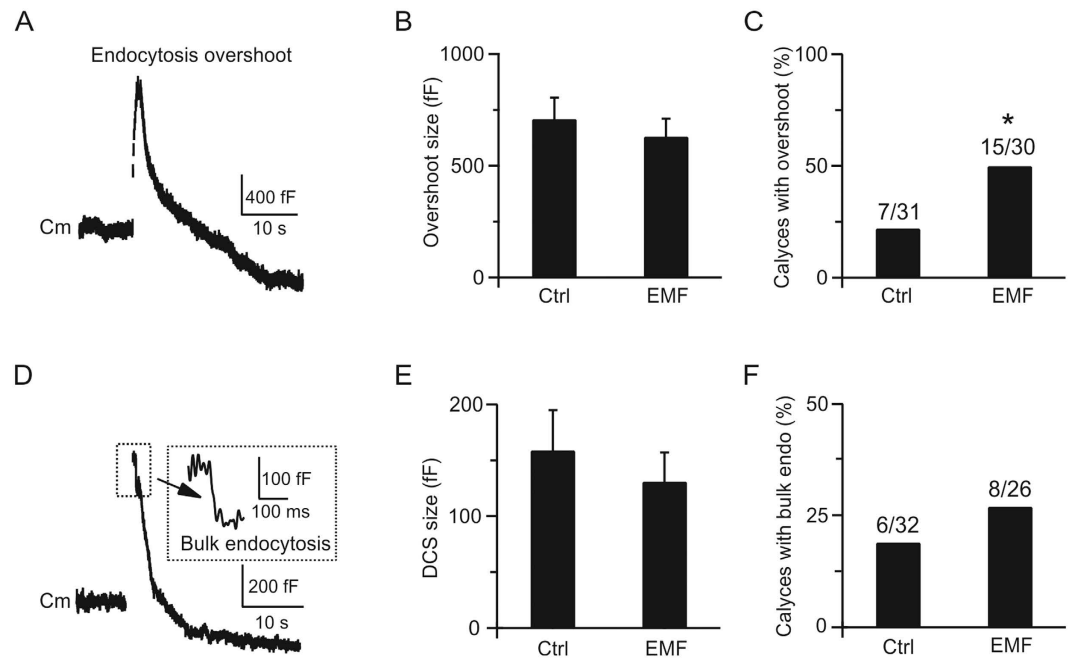


Figure 4. ELF-EMF exposure facilitates endocytosis overshoot and bulk endocytosis (A) Sampled Cm showing endocytosis overshoot induced by $\text{depol}_{50\text{ms} \times 10}$ with 5.5 mM extracellular calcium in controls. (B,C) Size and percentage of calyces showing endocytosis overshoot in the control (n = 31) and ELF-EMF groups (n = 30, *p < 0.05, chi-square test). (D) Sampled Cm showing bulk endocytosis induced by $\text{depol}_{50\text{ms} \times 10}$ with 5.5 mM extracellular calcium in controls. Inset, DCS in large scale. (E,F) Size and percentage of calyces showing bulk endocytosis overshoot in the control (n = 32) and ELF-EMF groups (n = 26).

a mean size of 131 ± 26 fF, which was similar to that of controls (p = 0.5, Fig. 4E,F). The proportion of calyces demonstrating bulk endocytosis after ELF-EMF exposure was only slightly higher than the proportion of controls (30% versus 18%) because the smaller calcium influx in mice during stimulation resulted in an even lower chance of detecting bulk endocytosis compared to rats. Nonetheless, the result was consistent with our hypothesis that a larger calcium influx increased the chance of detecting bulk endocytosis.

ELF-EMF potentiates post-tetanic potentiation. PTP, which is induced by a high-frequency train of action potential stimulation, has been reported at calyx of Held synapses as a form of short-term plasticity^{16,29,31,38}. The amplitude of the PTP, which is represented by the normalised maximum EPSC after the stimulation train, is calcium-dependent³¹. Longer stimulation train increases PTP, whereas EGTA-AM suppresses PTP^{16,31}. In the present study, we examined whether the increased influx of calcium caused by ELF-EMF exposure affects the PTP. First, we obtained a stable baseline of EPSCs by applying a brief stimulation (0.1 ms, 2–20 V) every 10 s for 300 s via a bipolar electrode positioned at the midline of the trapezoid body, and then applied a stimulation train at 100 Hz for 10 s ($\text{Train}_{10\text{s}}$), inducing a robust PTP of the EPSC^{16,29}. Shortly after the stimulation train, the EPSC amplitude was above baseline and peaked within 10–30 s (Fig. 5A,B). In controls, after the $\text{Train}_{10\text{s}}$, the EPSC reached a maximum of $190 \pm 13\%$ of baseline (n = 20), which was similar to our previous report (Fig. 5A)¹⁶. However, in the ELF-EMF exposure group, the PTP amplitude was $225 \pm 15\%$ after $\text{Train}_{10\text{s}}$ (n = 23, Fig. 5B,C), which is significantly higher than in controls (p < 0.05, Fig. 5D). This result is consistent with previous studies reporting that PTP is calcium-dependent and that longer stimulation train induced larger PTP¹⁶.

Although the increase in released vesicles dominate the peak of the PTP^{31,39}, compound vesicle fusion has also been reported to contribute to the slow component of the PTP^{16,29}. Here, two pieces of evidence ruled out this possibility after exposure to ELF-EMF: 1) we did not detect any mEPSC amplitude increase after ELF-EMF exposure (see Fig. 1), as compound fusion should increase mEPSC amplitude in parallel with the slow component of PTP^{16,29}, and 2) the slow component of the PTP decay after $\text{Train}_{10\text{s}}$ was not different between the two groups (control: $\tau = 112 \pm 12$ s, ELF-EMF group: $\tau = 114 \pm 20$ s, p = 0.8). Thus, we concluded that ELF-EMF potentiated the PTP by increasing the number of released vesicles but did not increase quantal size.

ELF-EMF increases the calcium channels at the presynaptic nerve terminal. We have shown that ELF-EMF increases calcium influx upon stimulation, accelerating all forms of endocytosis and potentiating PTP. However, the underlying mechanisms that facilitate the calcium influx are unknown. Since calcium influxes through the calcium channels at the presynaptic nerve terminal during depolarisation¹⁴, we examined calcium channel expression at the presynaptic nerve terminal using calcium channel-specific antibodies. Western blot showed that pan calcium channel expression was much higher in the ELF-EMF exposure group than in controls (normalised, $149 \pm 11\%$, n = 4, p < 0.05; Fig. 6A,C), which provided a structural guarantee for larger calcium influx during stimulation.

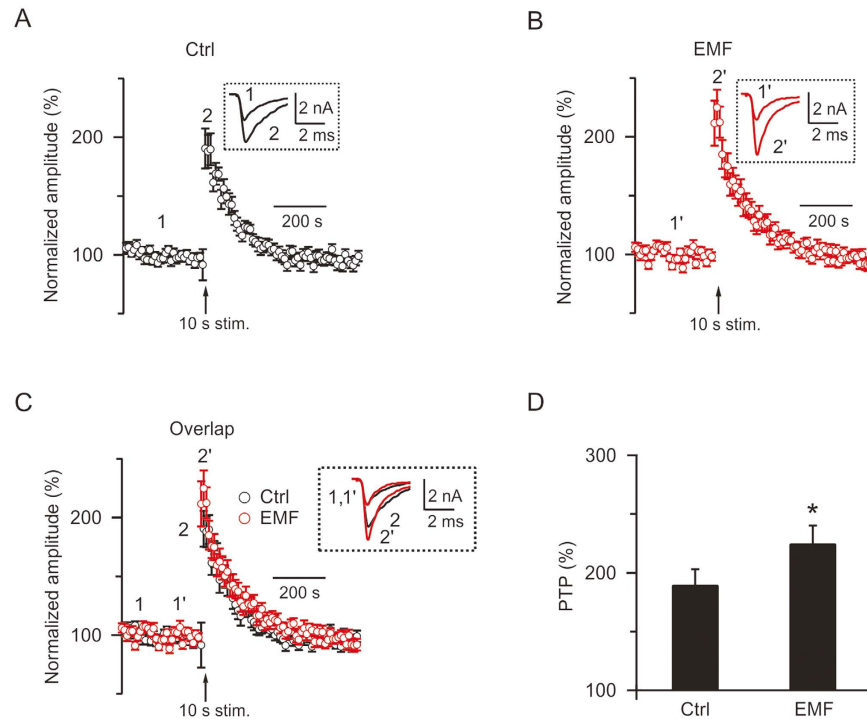


Figure 5. ELF-EMF potentiates post-tetanic potentiation (PTP) (A) Normalised EPSC amplitude change induced by a 100 Hz train for 10 s ($\text{Train}_{10\text{s}}$) in the control group ($n = 20$). The arrow indicates the time the $\text{Train}_{10\text{s}}$ was applied to induce PTP. Inset, sampled EPSC taken at times labelled. (B) Similar to A, but with the ELF-EMF exposure group ($n = 23$). (C) Similar to A and B, but with the control and ELF-EMF exposure groups in the same figure for comparison. (D) Amplitude of PTP (PTP%) in the control and ELF-EMF exposure groups (control: $190 \pm 13\%$; ELF-EMF group, $225 \pm 15\%$; $*p < 0.05$).

Three subtypes of calcium channels, P/Q, N, and R, are known to be expressed at the calyx of Held terminal^{40,41}. Therefore, we further examined the expression levels of all three subtypes of calcium channels at the calyx of Held nerve terminal (Fig. 6B). Western blots showed that all three subtypes of calcium channels are expressed at higher levels in the ELF-EMF exposure group compared to controls, though the R-type did not reach significance (P/Q: $169 \pm 12\%$, $n = 4$, $p < 0.01$; N: $124 \pm 7\%$, $n = 4$, $p < 0.05$; R: $110 \pm 4\%$, $n = 4$, $p = 0.07$; Fig. 6B,D), suggesting that all three subtypes could contribute to the acceleration of endocytosis and potentiation of PTP.

To investigate the mechanism underlying the increased expression of calcium channels at the presynaptic membrane after exposure to ELF-EMF, we used real-time PCR to examine the mRNA expression of the three subtypes of calcium channels (Fig. 6E). The relative mRNA expression levels of all three subtypes of calcium channels increased after exposure to ELF-EMF, though the R-type calcium channel did not reach significance (P/Q: $p < 0.01$; N: $p < 0.05$; R: $p = 0.08$; $n = 9$), suggesting that the increase in calcium channels at the presynaptic membrane was due to increased gene expression.

Previous studies have shown that the P/Q subtype calcium channel contributes 60–80% of the calcium current (N and R types contribute to less than 20% each)⁴² and dominates fast endocytosis at p8–p10 at calyx of Held synapses⁴³. Therefore, we concluded that the increased calcium channel expression at the presynaptic membrane, especially the P/Q subtype calcium channel, accounts for the facilitation of endocytosis and potentiation of PTP. The up-regulated expression of N and R type channels may also contribute to the acceleration of the slow component of vesicle endocytosis and help potentiate PTP.

Discussion

In this study, we report for the first time that exposure to ELF-EMF critically affects synaptic transmission and plasticity at calyx of Held synapses. With accurate presynaptic capacitance measurements, we provide direct evidence showing that exposure to ELF-EMF does not affect the RRP size during exocytosis, but dramatically accelerates all forms of vesicle endocytosis, including slow and rapid endocytosis, endocytosis overshoot, and bulk endocytosis (Figs 2–4). We also demonstrated that exposure to ELF-EMF potentiates synaptic transmission by increasing the amplitude of PTP, a form of short-term plasticity, but does not affect its time course^{44,45}. We further investigated the underlying mechanisms by which exposure to ELF-EMF affects synaptic transmission and found that the enhanced expression of calcium channels at the presynaptic nerve terminal, mostly the P/Q subtype, accounts for the increased calcium influx upon stimulation, facilitating vesicle endocytosis and synaptic plasticity. These findings show crucial regulatory roles of ELF-EMF in synaptic transmission and plasticity in the central nervous system.

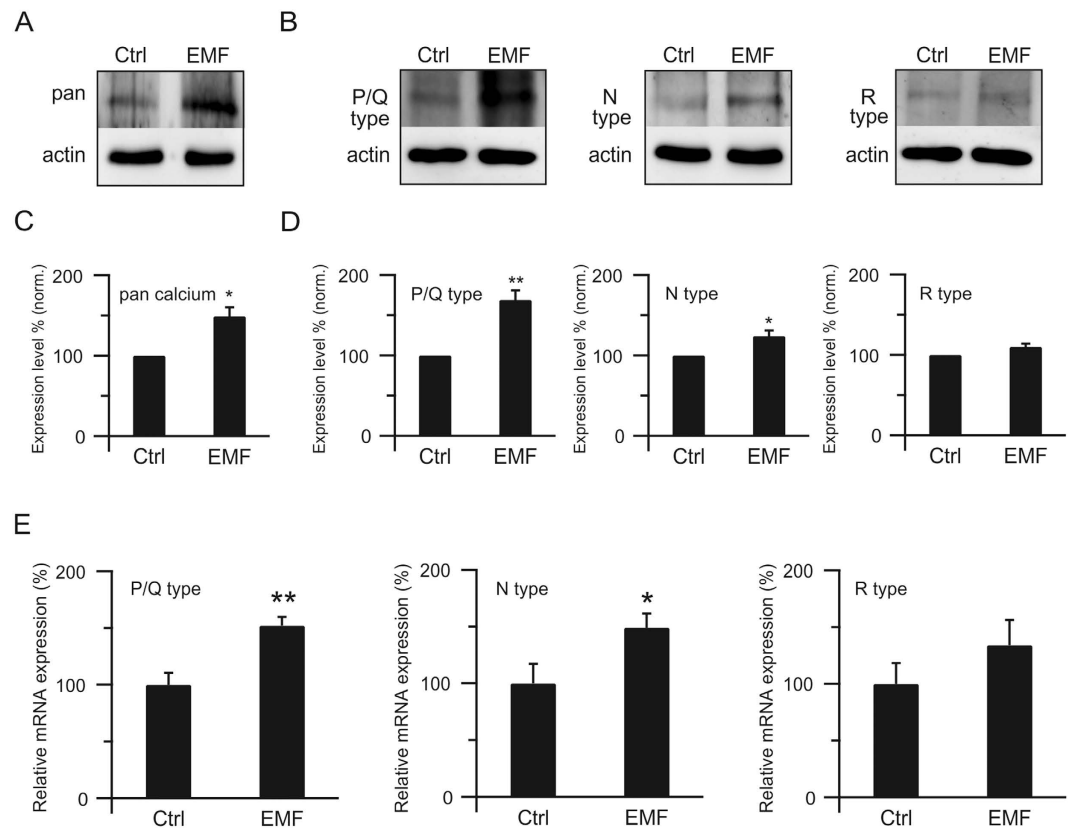


Figure 6. ELF-EMF increases calcium channels at the presynaptic nerve terminal (A) Western blot of pan calcium channel at the presynaptic terminal in the control (left) and ELF-EMF exposure groups (right). β -actin was used as a loading control. (B) Similar to A, but with P/Q (left), N (middle), and R (right) subtypes of calcium channels. (C) Expression level of pan calcium channel in the control (normalised) and ELF-EMF exposure groups ($n = 4$; ** $p < 0.01$). (D) Similar to C, but with P/Q (left), N (middle), and R (right) subtypes of calcium channels ($n = 4$ for each; ** $p < 0.01$; * $p < 0.05$). (E) Relative mRNA expression level of P/Q (left), N (middle), and R (right) subtypes of calcium channels (normalised to GAPDH, R subtype: $p = 0.08$; $n = 9$; ** $p < 0.01$; * $p < 0.05$).

Endocytosis, an essential biological event that retrieves vesicular membrane and proteins, is important in preventing cells from swelling or shrinking and in maintaining synaptic transmission by preventing the depletion of synaptic vesicles^{13,22}. Despite such important roles, studies regarding the effects of exposure to ELF-EMF on this cellular event are rare and controversial¹⁷. 50-Hz magnetic fields at 1 mT significantly stimulated the phagocytic activity of differentiated murine macrophages whereas 60-Hz magnetic fields resulted in no significant differences in the phagocytosis of *Candida albicans* by peritoneal murine macrophages^{46,47}. Inhibitors of clathrin-dependent endocytosis were also reported to prevent the increase in endocytosis provoked by GSM-EMF (mobile phone EMF in particular) signals¹⁷. In the present study, we investigated the effects of ELF-EMF exposure on endocytosis in brain slices. All forms of endocytosis are accurately evaluated by direct capacitance measurements. Our findings suggest facilitation of all forms of endocytosis due to an increase in calcium influx.

Synaptic plasticity is important in neuronal circuit function⁴⁸. PTP, a short-term plasticity of minutes induced by a high-frequency train of action potential stimulation, has been observed in calyces^{16,29,39}. This form of short-term plasticity is reported to be calcium-dependent, which increases the number of vesicles released^{38,39,49}. In the present study, we found that the increased influx of calcium also potentiates PTP (Fig. 5C). We previously showed that compound fusion between vesicles accounts for the mEPSC increase and slow component of PTP after the stimulation train^{16,29}. As neither the increase in mEPSC amplitude nor changes in the slow component of PTP were observed after exposure to ELF-EMF, we concluded that compound fusion is not affected by ELF-EMF, which is consistent with the lack of changes in RRP size and exocytosis.

The biological effects of electromagnetic fields, especially the extremely low frequency fields, have been studied for more than fifty years and a huge amount of evidence has accumulated regarding the possible effects of ELF-EMF on living system⁹, including cancer⁵⁰⁻⁵², immune cells^{53,54}, bone cells⁵⁵, and nerve cells^{30,56,57}. However, there is still no general agreement on the relevant underlying mechanisms. Calcium, which acts as a messenger in many intracellular processes, such as differentiation, proliferation, and apoptosis, is strictly regulated in almost all cell types⁵⁸, and many studies have shown that voltage-dependent calcium channels may account for the biological effects after exposure to EMF, such that calcium channel blockers could greatly lower the effects of ELF-EMF exposure⁵⁹. It is well established that calcium triggers exocytosis and also we recently reported calcium initiates all forms of endocytosis¹⁸. Thus, our findings that the enhanced calcium channel expression, especially of the P/Q

subtype, accelerates vesicle endocytosis and potentiates PTP may provide a new mechanism for how ELF-EMF regulates synaptic transmission at the cellular level in the central nervous system. The acceleration of endocytosis may facilitate synaptic strength, which may further regulate neuronal development, axonal branching, and refinement. The potentiation of PTP may also lead to strengthening the connection between neurons, which may further bolster the neuronal circuits^{13,48}. Furthermore, enhanced calcium channel expression, especially of the P/Q subtype, after exposure to ELF-EMF may link many regulatory pathways that are calcium-dependent, such as the PKC pathway^{29,39} and calcium/calmodulin/calcineurin pathway^{18,20}, which could induce more downstream regulatory factors. As efficient exo-endocytosis recycling is essential for brain function¹³, our findings may also offer new therapeutic insights for neurological disorders⁶⁰.

How exposure to ELF-EMF increases more calcium channels at the presynaptic nerve terminal, and how these newly expressed channels are located in the right place at the active zone to trigger calcium influx upon stimulation are key questions that remain to be solved. Moreover, whether other proteins, such as SNARE proteins and synaptotagmin, are required during this process is still unknown. Understanding these questions would be of great interest in the future and help us resolve the details of the mechanisms underlying ELF-EMF-regulated neuronal communication.

References

- Juutilainen, J. Developmental effects of electromagnetic fields. *Bioelectromagnetics* Suppl 7, S107–115, doi: 10.1002/bem.20125 (2005).
- Zalata, A., El-Samanoudy, A. Z., Shaalan, D., El-Baiomy, Y. & Mostafa, T. *In vitro* effect of cell phone radiation on motility, DNA fragmentation and clusterin gene expression in human sperm. *Int J Fertil Steril* 9, 129–136 (2015).
- Pesce, M., Patruno, A., Speranza, L. & Reale, M. Extremely low frequency electromagnetic field and wound healing: implication of cytokines as biological mediators. *Eur Cytokine Netw* 24, 1–10, doi: 10.1684/ecn.2013.0332 (2013).
- Sandyk, R. Brief communication: electromagnetic fields improve visuospatial performance and reverse agraphia in a parkinsonian patient. *Int J Neurosci* 87, 209–217 (1996).
- Zhang, Y., Liu, X., Zhang, J. & Li, N. Short-term effects of extremely low frequency electromagnetic fields exposure on Alzheimer's disease in rats. *Int J Radiat Biol* 91, 28–34, doi: 10.3109/09553002.2014.954058 (2015).
- Ramundo-Orlando, A., Mattia, F., Palombo, A. & D'Inzeo, G. Effect of low frequency, low amplitude magnetic fields on the permeability of cationic liposomes entrapping carbonic anhydrase: II. No evidence for surface enzyme involvement. *Bioelectromagnetics* 21, 499–507 (2000).
- Marchionni, I. *et al.* Comparison between low-level 50 Hz and 900 MHz electromagnetic stimulation on single channel ionic currents and on firing frequency in dorsal root ganglion isolated neurons. *Biochim Biophys Acta* 1758, 597–605, doi: 10.1016/j.bbame.2006.03.014 (2006).
- Grassi, C. *et al.* Effects of 50 Hz electromagnetic fields on voltage-gated Ca²⁺ channels and their role in modulation of neuroendocrine cell proliferation and death. *Cell Calcium* 35, 307–315, doi: 10.1016/j.ceca.2003.09.001 (2004).
- Santini, M. T., Rainaldi, G. & Indovina, P. L. Cellular effects of extremely low frequency (ELF) electromagnetic fields. *Int J Radiat Biol* 85, 294–313, doi: 10.1080/09553000902781097 (2009).
- Gavoci, E. *et al.* ELF magnetic fields tuned to ion parametric resonance conditions do not affect TEA-sensitive voltage-dependent outward K(+) currents in a human neural cell line. *Bioelectromagnetics* 34, 579–588, doi: 10.1002/bem.21807 (2013).
- Mathie, A., Kennard, L. E. & Veale, E. L. Neuronal ion channels and their sensitivity to extremely low frequency weak electric field effects. *Radiat Prot Dosimetry* 106, 311–316 (2003).
- Saunders, R. D. & Jefferys, J. G. A neurobiological basis for ELF guidelines. *Health Phys* 92, 596–603, doi: 10.1097/01.HP0000257856.83294.3e (2007).
- Wu, L. G., Hamid, E., Shin, W. & Chiang, H. C. Exocytosis and endocytosis: modes, functions, and coupling mechanisms. *Annu Rev Physiol* 76, 301–331, doi: 10.1146/annurev-physiol-021113-170305 (2014).
- Xue, L. *et al.* Voltage-dependent calcium channels at the plasma membrane, but not vesicular channels, couple exocytosis to endocytosis. *Cell reports* 1, 632–638, doi: 10.1016/j.celrep.2012.04.011 (2012).
- Guo, J. *et al.* A three-pool model dissecting readily releasable pool replenishment at the calyx of held. *Sci Rep* 5, 9517, doi: 10.1038/srep09517 (2015).
- He, L. *et al.* Compound vesicle fusion increases quantal size and potentiates synaptic transmission. *Nature* 459, 93–97, doi: 10.1038/nature07860 (2009).
- Moisescu, M. G., Leveque, P., Verjus, M. A., Kovacs, E. & Mir, L. M. 900 MHz modulated electromagnetic fields accelerate the clathrin-mediated endocytosis pathway. *Bioelectromagnetics* 30, 222–230, doi: 10.1002/bem.20463 (2009).
- Wu, X. S. *et al.* Ca(2+) and calmodulin initiate all forms of endocytosis during depolarization at a nerve terminal. *Nat Neurosci* 12, 1003–1010, doi: 10.1038/nn.2355 (2009).
- Wu, W., Xu, J., Wu, X. S. & Wu, L. G. Activity-dependent acceleration of endocytosis at a central synapse. *J Neurosci* 25, 11676–11683 (2005).
- Xue, L. *et al.* A membrane pool retrieved via endocytosis overshoot at nerve terminals: a study of its retrieval mechanism and role. *J Neurosci* 32, 3398–3404, doi: 10.1523/JNEUROSCI.5943-11.2012 (2012).
- Wu, W. & Wu, L. G. Rapid bulk endocytosis and its kinetics of fission pore closure at a central synapse. *Proc.Natl.Acad.Sci.USA* 104, 10234–10239 (2007).
- Wu, L. G., Ryan, T. A. & Lagnado, L. Modes of vesicle retrieval at ribbon synapses, calyx-type synapses, and small central synapses. *J.Neurosci.* 27, 11793–11802 (2007).
- Fanelli, C. *et al.* Magnetic fields increase cell survival by inhibiting apoptosis via modulation of Ca²⁺ influx. *FASEB journal: official publication of the Federation of American Societies for Experimental Biology* 13, 95–102 (1999).
- Barbier, E., Dufy, B. & Veyret, B. Stimulation of Ca²⁺ influx in rat pituitary cells under exposure to a 50 Hz magnetic field. *Bioelectromagnetics* 17, 303–311, doi: 10.1002/(SICI)1521-186X(1996)17:4<303::AID-BEM6>3.0.CO;2-7 (1996).
- Lyle, D. B., Fuchs, T. A., Casamento, J. P., Davis, C. C. & Swicord, M. L. Intracellular calcium signaling by Jurkat T-lymphocytes exposed to a 60 Hz magnetic field. *Bioelectromagnetics* 18, 439–445 (1997).
- Wey, H. E., Conover, D. P., Mathias, P., Torason, M. & Lotz, W. G. 50-Hertz magnetic field and calcium transients in Jurkat cells: results of a research and public information dissemination (RAPID) program study. *Environ Health Perspect* 108, 135–140 (2000).
- Madec, F., Billaudel, B., Charlet de Sauvage, R., Sartor, P. & Veyret, B. Effects of ELF and static magnetic fields on calcium oscillations in islets of Langerhans. *Bioelectrochemistry* 60, 73–80 (2003).
- Craviso, G. L. *et al.* Intracellular calcium activity in isolated bovine adrenal chromaffin cells in the presence and absence of 60 Hz magnetic fields. *Bioelectromagnetics* 23, 557–567, doi: 10.1002/bem.10045 (2002).
- Xue, L. & Wu, L. G. Post-tetanic potentiation is caused by two signalling mechanisms affecting quantal size and quantal content. *J Physiol* 588, 4987–4994, doi: 10.1113/jphysiol.2010.196964 (2010).

30. He, Y. L. *et al.* Exposure to extremely low-frequency electromagnetic fields modulates Na⁺ currents in rat cerebellar granule cells through increase of AA/PGE2 and EP receptor-mediated cAMP/PKA pathway. *PLoS one* **8**, e54376, doi: 10.1371/journal.pone.0054376 (2013).
31. Korogod, N., Lou, X. & Schneggenburger, R. Presynaptic Ca²⁺ requirements and developmental regulation of posttetanic potentiation at the calyx of Held. *J Neurosci* **25**, 5127–5137 (2005).
32. Han, Y. *et al.* Basis of aggravated hepatic lipid metabolism by chronic stress in high-fat diet-fed rat. *Endocrine* **48**, 483–492, doi: 10.1007/s12020-014-0307-x (2015).
33. Rizzoli, S. O. & Betz, W. J. Synaptic vesicle pools. *Nat. Rev. Neurosci.* **6**, 57–69 (2005).
34. Xu, J. *et al.* GTP-independent rapid and slow endocytosis at a central synapse. *Nat. Neurosci.* **11**, 45–53 (2008).
35. Hosoi, N., Holt, M. & Sakaba, T. Calcium dependence of exo- and endocytotic coupling at a glutamatergic synapse. *Neuron* **63**, 216–229, doi: 10.1016/j.neuron.2009.06.010 (2009).
36. Smith, C. & Neher, E. Multiple forms of endocytosis in bovine adrenal chromaffin cells. *J. Cell Biol.* **139**, 885–894 (1997).
37. Richards, D. A., Guatimosim, C. & Betz, W. J. Two endocytic recycling routes selectively fill two vesicle pools in frog motor nerve terminals. *Neuron* **27**, 551–559 (2000).
38. Xu, J., He, L. & Wu, L. G. Role of Ca(2+) channels in short-term synaptic plasticity. *Curr. Opin. Neurobiol.* **17**, 352–359 (2007).
39. Korogod, N., Lou, X. & Schneggenburger, R. Posttetanic potentiation critically depends on an enhanced Ca(2+) sensitivity of vesicle fusion mediated by presynaptic PKC. *Proc Natl Acad Sci USA* **104**, 15923–15928, doi: 10.1073/pnas.0704603104 (2007).
40. Wu, L. G., Westenbroek, R. E., Borst, J. G. G., Catterall, W. A. & Sakmann, B. Calcium channel types with distinct presynaptic localization couple differentially to transmitter release in single calyx-type synapses. *J. Neurosci.* **19**, 726–736 (1999).
41. Thanawala, M. S. & Regehr, W. G. Presynaptic calcium influx controls neurotransmitter release in part by regulating the effective size of the readily releasable pool. *J Neurosci* **33**, 4625–4633, doi: 10.1523/JNEUROSCI.4031-12.2013 (2013).
42. Iwasaki, S., Momiyama, A., Uchitel, O. D. & Takahashi, T. Developmental changes in calcium channel types mediating central synaptic transmission. *J. Neurosci.* **20**, 59–65 (2000).
43. Midorikawa, M., Okamoto, Y. & Sakaba, T. Developmental changes in Ca²⁺ channel subtypes regulating endocytosis at the calyx of Held. *J Physiol* **592**, 3495–3510, doi: 10.1113/jphysiol.2014.273243 (2014).
44. von Gersdorff, H. & Borst, J. G. Short-term plasticity at the calyx of Held. *Nature reviews. Neuroscience* **3**, 53–64, doi: 10.1038/nrn705 (2002).
45. Regehr, W. G. Short-term presynaptic plasticity. *Cold Spring Harbor perspectives in biology* **4**, a005702, doi: 10.1101/cshperspect.a005702 (2012).
46. Frahm, J., Lantow, M., Lupke, M., Weiss, D. G. & Simko, M. Alteration in cellular functions in mouse macrophages after exposure to 50 Hz magnetic fields. *J Cell Biochem* **99**, 168–177, doi: 10.1002/jcb.20920 (2006).
47. Jacobi-Elizondo, J. S., Gomez-Flores, R., Tamez-Guerra, R., Rodriguez-Padilla, C. & Heredia-Rojas, J. A. Acute effects of 60-Hz electromagnetic fields on *ex vivo* murine lymphocyte and macrophage functions, and *in vitro* tumor cell growth. *Rev Latinoam Microbiol* **43**, 130–134 (2001).
48. Abbott, L. F. & Regehr, W. G. Synaptic computation. *Nature* **431**, 796–803 (2004).
49. Habets, R. L. & Borst, J. G. Post-tetanic potentiation in the rat calyx of Held synapse. *J Physiol* **564**, 173–187 (2005).
50. Ahlbom, A. *et al.* A pooled analysis of magnetic fields and childhood leukaemia. *Br J Cancer* **83**, 692–698, doi: 10.1054/bjoc.2000.1376 (2000).
51. Greenland, S., Sheppard, A. R., Kaune, W. T., Poole, C. & Kelsh, M. A. A pooled analysis of magnetic fields, wire codes, and childhood leukemia. Childhood Leukemia-EMF Study Group. *Epidemiology* **11**, 624–634 (2000).
52. McBride, M. L. *et al.* Power-frequency electric and magnetic fields and risk of childhood leukemia in Canada. *Am J Epidemiol* **149**, 831–842 (1999).
53. Nindl, G. *et al.* Experiments showing that electromagnetic fields can be used to treat inflammatory diseases. *Biomed Sci Instrum* **36**, 7–13 (2000).
54. McCreary, C. R., Dixon, S. J., Fraher, L. J., Carson, J. J. & Prato, F. S. Real-time measurement of cytosolic free calcium concentration in Jurkat cells during ELF magnetic field exposure and evaluation of the role of cell cycle. *Bioelectromagnetics* **27**, 354–364, doi: 10.1002/bem.20248 (2006).
55. Selvamurugan, N., Kwok, S., Vasilov, A., Jefcoat, S. C. & Partridge, N. C. Effects of BMP-2 and pulsed electromagnetic field (PEMF) on rat primary osteoblastic cell proliferation and gene expression. *J Orthop Res* **25**, 1213–1220, doi: 10.1002/jor.20409 (2007).
56. Cui, Y., Liu, X., Yang, T., Mei, Y. A. & Hu, C. Exposure to extremely low-frequency electromagnetic fields inhibits T-type calcium channels via AA/LTE4 signaling pathway. *Cell Calcium* **55**, 48–58, doi: 10.1016/j.ceca.2013.11.002 (2014).
57. Lai, H. & Carino, M. 60 Hz magnetic fields and central cholinergic activity: effects of exposure intensity and duration. *Bioelectromagnetics* **20**, 284–289 (1999).
58. Berridge, M. J., Lipp, P. & Bootman, M. D. The versatility and universality of calcium signalling. *Nature reviews. Molecular cell biology* **1**, 11–21, doi: 10.1038/35036035 (2000).
59. Pall, M. L. Electromagnetic fields act via activation of voltage-gated calcium channels to produce beneficial or adverse effects. *Journal of cellular and molecular medicine* **17**, 958–965, doi: 10.1111/jcmm.12088 (2013).
60. Reale, M. *et al.* Neuronal cellular responses to extremely low frequency electromagnetic field exposure: implications regarding oxidative stress and neurodegeneration. *PLoS one* **9**, e104973, doi: 10.1371/journal.pone.0104973 (2014).

Acknowledgements

This work was sponsored by the National Basic Research Program of China (2011CB503703), National High-tech R&D Program of China (2015AA020512), National Natural Science Foundation of China (grant number: 31370828 and 31570833), Specialised Research Fund for the Doctoral Program of Higher Education (SRFDPF, grant number: 20120071120013), and the Shanghai Leading Academic Discipline Project (B111).

Author Contributions

Z.-C.S., J.G., Y.F. and L.X. designed the research; Z.-C.S., J.-L.G. and J.G. performed the electrophysiological experiments; Y.F. and B.G. performed the Western blot and real-time PCR experiments; M.H., Y.-C.W., T.L., Y.-A.L., P.-T.Y. and Y.-A.M. helped with experiments; L.X. supervised the project and wrote the paper.

Additional Information

Supplementary information accompanies this paper at <http://www.nature.com/srep>

Competing financial interests: The authors declare no competing financial interests.

How to cite this article: Sun, Z. *et al.* Extremely Low Frequency Electromagnetic Fields Facilitate Vesicle Endocytosis by Increasing Presynaptic Calcium Channel Expression at a Central Synapse. *Sci. Rep.* **6**, 21774; doi: 10.1038/srep21774 (2016).



This work is licensed under a Creative Commons Attribution 4.0 International License. The images or other third party material in this article are included in the article's Creative Commons license, unless indicated otherwise in the credit line; if the material is not included under the Creative Commons license, users will need to obtain permission from the license holder to reproduce the material. To view a copy of this license, visit <http://creativecommons.org/licenses/by/4.0/>



OPEN

SUBJECT AREAS:

SYNAPTIC VESICLE
ENDOCYTOSIS

SHORT-TERM POTENTIATION

Received

2 December 2014

Accepted

6 March 2015

Published

31 March 2015

Correspondence and
requests for materials
should be addressed to
L.X. (lxue@fudan.edu.
cn)

* These authors
contributed equally to
this work.

A Three-Pool Model Dissecting Readily Releasable Pool Replenishment at the Calyx of Held

Jun Guo^{1*}, Jian-long Ge^{1*}, Mei Hao^{1*}, Zhi-cheng Sun^{1*}, Xin-sheng Wu², Jian-bing Zhu¹, Wei Wang¹, Pan-tong Yao¹, Wei Lin³ & Lei Xue¹

¹State Key Laboratory of Genetic Engineering, Collaborative Innovation Center of Genetics and Development, Department of Physiology and Biophysics, School of Life Sciences, Fudan University, Shanghai, P.R. China, 200433, ²Synaptic Transmission Section, National Institute of Neurological Disorders and Stroke, Bethesda, Maryland, 20892, ³School of Mathematical Sciences, Centre for Computational Systems Biology and Shanghai Centre for Mathematical Sciences, Fudan University, P.R.China, 200433.

Although vesicle replenishment is critical in maintaining exo-endocytosis recycling, the underlying mechanisms are not well understood. Previous studies have shown that both rapid and slow endocytosis recycle into a very large recycling pool instead of within the readily releasable pool (RRP), and the time course of RRP replenishment is slowed down by more intense stimulation. This finding contradicts the calcium/calmodulin-dependence of RRP replenishment. Here we address this issue and report a three-pool model for RRP replenishment at a central synapse. Both rapid and slow endocytosis provide vesicles to a large reserve pool (RP) ~ 42.3 times the RRP size. When moving from the RP to the RRP, vesicles entered an intermediate pool (IP) ~ 2.7 times the RRP size with slow RP-IP kinetics and fast IP-RRP kinetics, which was responsible for the well-established slow and rapid components of RRP replenishment. Depletion of the IP caused the slower RRP replenishment observed after intense stimulation. These results establish, for the first time, a realistic cycling model with all parameters measured, revealing the contribution of each cycling step in synaptic transmission. The results call for modification of the current view of the vesicle recycling steps and their roles.

Repetitive firing causes short-term depression (STD) at many synapses¹, which plays an important computational role in neuronal circuits². A major mechanism underlying STD during intense stimulation is depletion of the readily releasable pool (RRP)¹. The degree of RRP depletion and its subsequent replenishment may determine the degree and the time course of STD, and thus the synaptic strength and neuronal circuit function¹. Given such important roles, however, the source of vesicles that are mobilised to replenish the RRP and the mechanism that determines the rate of the RRP replenishment remain poorly understood.

Studies several decades ago revealed that intense stimulation slows the recovery of STD³. Accordingly, a vesicle cycling model composed of two pools, the RRP and the reserve pool (RP: containing all vesicles except those in the RRP) was proposed, in which fused vesicles are retrieved via endocytosis to the RP, which then supplies vesicles to the RRP. Depletion of the RP could thus account for the slower recovery of STD^{1,3}. Consistent with this model, blocking endocytosis at the neuromuscular junction of *shibire* mutants led to a progressive decline in transmitter release during repetitive stimulation^{4,5}. However, this model has not been tested rigorously by measuring all model parameters, including pool sizes, RP-RRP kinetics, and endocytosis rates, and by determining whether the model with measured parameters matches the observed STD. More importantly, many additional factors have been reported since this model was proposed, including various forms of endocytosis, vesicle pools, and various rates of the RRP replenishment, which necessitates a rethinking the model.

Studies in the last 15 years have revealed that endocytosis can be rapid (1–2 s) or slow (10–30 s)^{6,7}. Rapid endocytosis is often considered to be kiss-and-run fusion and retrieval⁸, which involves rapid fusion pore opening and closure at the same site^{9–12}. It has been proposed that kiss-and-run locally recycles vesicles within the RRP at cultured hippocampal synapses^{13–15}, though whether rapid kiss-and-run exists at this synapse is still debated⁸.

Slow endocytosis, mediated by a clathrin-dependent mechanism^{16,17}, is considered a major endocytic pathway¹⁷. This pathway is hypothesised to retrieve vesicles into a small recycling pool¹⁸. The concept of a small recycling pool was based on the finding that only a small fraction (~ 5 –20%) of vesicles can be stained with the



styryl dye (e.g., FM1-43) during low and intermediate frequency stimulation that releases all recycling vesicles¹⁸. If this concept holds, two predictions can be made: 1) the majority of vesicles residing in the RP are irrelevant to synaptic transmission under many physiological conditions, and 2) interference of this small recycling pool will have a crucial and rapid influence on the RRP replenishment. However, our previous studies challenged the presence of a small recycling pool. First, by simultaneously recording presynaptic capacitance and postsynaptic EPSC in the absence or presence of glutamate at rat calyces, we suggest a large recycling pool ~ 46 times the size of RRP, which is close to the total vesicle amount measured by electron microscopy^{19,20}. Such a large recycling pool confirms that almost all vesicles are mobilised to maintain synaptic transmission upon high frequency stimulation²⁰. Second, we have shown that blocking of both rapid and slow endocytosis does not affect the rate of RRP replenishment²¹, which rules out the possibility that endocytosed vesicles recycle within the RRP or a small recycling pool because it predicts slower RRP replenishment when endocytosis is blocked. Therefore, our previous results suggest that endocytosed vesicles are retrieved into a large recycling pool instead of a small one.

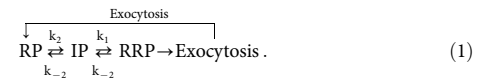
The RRP replenishment time course is often bi-exponential with a calcium/calmodulin-dependent rapid component of ~ 1 s or less^{22–25}. However, the source of vesicles responsible for rapid and slow RRP replenishment is unclear. Original candidates that were considered include vesicles formed by rapid endocytosis and the small recycling pool¹⁸. However, both candidates have been ruled out based on our previous studies^{20,21}. Furthermore, we found that the RRP replenishment time course was slowed down by more intense stimulation²¹. Since the RRP replenishment is calcium/calmodulin-dependent, stronger stimulation should increase the intracellular calcium concentration, and facilitate calmodulin function to speed up the RRP replenishment^{23,25}. Thus, a mechanism other than calcium/calmodulin regulation must be involved.

Here, we provide a realistic three-pool model with all parameters experimentally measured, which shows the contribution of each step in exo- and endocytosis, and explains why the RRP replenishment is composed of rapid and slow components, and why the RRP replenishment could be slowed down by intense stimulation. We further applied this model to evaluate the contribution of endocytosis under prolonged action potential-like stimulation train. The current view of vesicle cycling may need to be modified to include the large recycling pool²⁰ and the new intermediate pool in order to accommodate these new findings.

Methods

Slice preparation and electrophysiology. Slice preparation was similar as described previously^{7,26,27}. Briefly, Postnatal day 7–10 (p7–p10) old Wistar rats of either sex were decapitated and the brain stem slices of ~ 200 μm thick containing the medial nucleus of the trapezoid body (MNTB) were prepared using a vibratome (VT 1200s, Leica, Germany). Recordings were made at room temperature (22–24°C). Whole-cell capacitance measurements were made with the EPC-10 amplifier together with the software lock-in amplifier (PatchMaster, HEKA, Lambrecht, Germany). Exocytosis and endocytosis are represented by capacitance changes after conditioning stimulation^{20,27}. Measurements of the RRP size and RRP replenishment time course were similar to previous reports^{21,26}. The presynaptic pipette (3.5–5 M Ω) solution contained (in mM): 125 Cs-gluconate, 20 CsCl, 4 MgATP, 10 Na₂-phosphocreatine, 0.3 GTP, 10 HEPES, 0.05 BAPTA (pH 7.2, adjusted with CsOH). Measurements of the AMPA receptor-mediated EPSC were made by whole-cell patch at the postsynaptic principle neurons. The postsynaptic pipette (2.5–4 M Ω) solution contained (in mM): 125 K-gluconate, 20 KCl, 4 Mg-ATP, 10 Na₂-phosphocreatine, 0.3 GTP, 10 HEPES, and 0.5 EGTA (pH 7.2, adjusted with KOH). The series resistance (< 10 M Ω) was compensated by 90% (lag 10 μs). For recordings of the EPSC, kynurenic acid (1 mM) was added in the bath solution to relieve saturation and desensitisation of postsynaptic AMPA receptors. The holding potential was -80 mV for both presynaptic and postsynaptic recordings if not mentioned. Statistical analysis used a t test unless otherwise noted, and means are presented as \pm SE. All the methods were carried out in accordance with the approved guidelines and all animal experimental protocols were approved by the Animal Care and Use Committee of Fudan University.

Three-pool vesicle cycling model. With a large recycling pool ~ 46 times the size of RRP, we could not find any existing two-pool model that can fit the bi-exponential RRP replenishment with the rapid component being reduced by more intense stimulus^{20,21}. We proposed a new model composed of three vesicle pools, a reserve pool (RP), an intermediate pool (IP) between the RP and the RRP, and a RRP with reversible first order kinetics between RP and IP (k_2, k_{-2}) and between the IP and RRP (k_1, k_{-1}). The kinetic scheme for these three pools is:



Endocytosed vesicles enter only the RP, not the IP or RRP²¹, and the percentage of rapid and slow endocytosis was from our previous study²⁷. As blocking endocytosis does not affect RRP replenishment²¹, to simplify the mathematical reasoning, we did not include the endocytosed vesicles when calculating all of the parameters and included them back using MATLAB Simbiology toolbox (v2014a, The Mathworks, USA) to generate the vesicle cycling in each time step. The simplified scheme is shown below:



This model could explain the bi-exponential time course of replenishment by assuming a rapid rate constant for k_1 and k_{-1} , a slow rate constant for k_2 and k_{-2} , and a small IP size. The small IP could be depleted more by a more intense stimulus, explaining why the replenishment_{rapid} amplitude was decreased, instead of increased, after more intense stimulation. In the following, we performed quantitative calculations to determine the parameters (initial size of IP, RP, and k_1, k_{-1}, k_2 , and k_{-2}) that fit our data.

From scheme 2,

$$d\text{IP}/dt = k_2 * \text{RP} - k_{-2} * \text{IP} - k_1 * \text{IP} + k_{-1} * \text{RRP}, \quad (3)$$

where RP, IP, and RRP are the corresponding amount at time t after stimulation.

$$d\text{RRP}/dt = k_1 * \text{IP} - k_{-1} * \text{RRP} \quad (4)$$

From the law of conservation of mass,

$$\text{RP}_\infty - \text{RP} + \text{IP}_\infty - \text{IP} = \text{RRP}, \quad (5)$$

where ∞ denotes the steady state, or the resting condition. (We assumed them the same here to simplify calculation.)

Based on equations 3–5, we obtained the second order differential equation of RRP:

$$\frac{d^2\text{RRP}}{dt^2} + (k_1 + k_{-1} + k_2 + k_{-2}) * \frac{d\text{RRP}}{dt} + (k_1 + k_2 + k_2 * k_{-1} + k_{-1} * k_{-2}) * \text{RRP} - k_1 * k_2 * (\text{RP}_\infty + \text{IP}_\infty) = 0. \quad (6)$$

The solution of this differential equation is:

$$\text{RRP} = A_1 * \left(1 - e^{-\frac{t}{\tau_1}}\right) + A_2 * \left(1 - e^{-\frac{t}{\tau_2}}\right), \quad (7)$$

where

$$\tau_1 = \left[\frac{-\frac{1}{2} * k_2 - \frac{1}{2} * k_1 - \frac{1}{2} * k_{-2} - \frac{1}{2} * k_{-1} - \frac{1}{2} * (k_2^2 - 2 * k_1 * k_2 + 2 * k_2 * k_{-2})}{-2 * k_2 * k_{-1} + k_1^2 + 2 * k_1 * k_{-2} + 2 * k_1 * k_{-1} + k_2^2 - 2 * k_{-2} * k_{-1} + k_{-1}^2} \right]^{-1}, \quad (8)$$

$$\tau_2 = \left[\frac{-\frac{1}{2} * k_2 - \frac{1}{2} * k_1 - \frac{1}{2} * k_{-2} - \frac{1}{2} * k_{-1} + \frac{1}{2} * (k_2^2 - 2 * k_1 * k_2 + 2 * k_2 * k_{-2})}{-2 * k_2 * k_{-1} + k_1^2 + 2 * k_1 * k_{-2} + 2 * k_1 * k_{-1} + k_2^2 - 2 * k_{-2} * k_{-1} + k_{-1}^2} \right]^{-1}, \quad (9)$$

$$A_1 = \left(-A_2 * k_2 * k_1 - A_2 * k_2 * k_{-1} - A_2 * k_{-2} * k_{-1} + k_2 * k_1 * \text{RP}_\infty + k_2 * k_1 * \text{IP}_\infty \right) * (k_2 * k_1 + k_2 * k_{-1} + k_{-2} * k_{-1})^{-1}, \quad (10)$$

and A_2 is a constant (the integral constant).

Based on equation 7, at the steady state ($t = \infty$), $\text{RRP}_\infty = A_1 + A_2$. For simplicity, we normalised the RRP_∞ to 1. Thus,

$$A_2 = 1 - A_1. \quad (11)$$

Equation 7 indicates that the RRP replenishment time course is bi-exponential. Equations 8–9 indicate that the time constants for both rapid and slow RRP are independent of the stimulation intensity but depend on only four kinetic constants, k_1, k_{-1}, k_2 , and k_{-2} . These features are consistent with our experimental result that the RRP replenishment time course is bi-exponential, and that the time constants for rapid and slow RRP replenishment did not change significantly after 1–10 pulses of 20 ms depolarisation (Fig. 1). Such a consistency further strengthened our model.

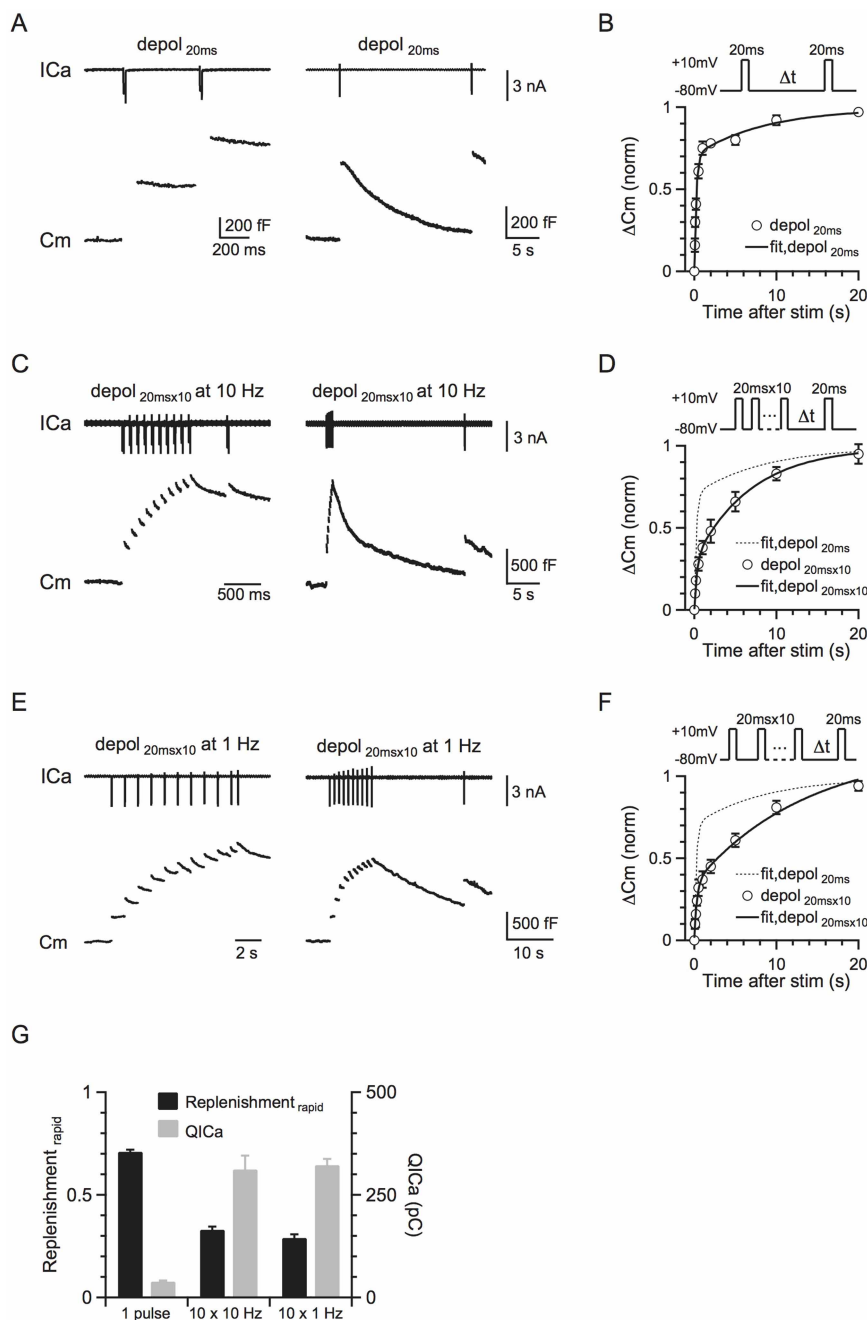


Figure 1 | More intense stimulation slows the RRP replenishment. (A) Left: Sampled presynaptic calcium current (ICa, upper) and membrane capacitance (Cm, lower) induced by a 20 ms depolarisation followed by a conditioning pulse of 20 ms depolarization with a 0.5 s interval. Right: Similar to Left, except that the stimulus interval is 20 s. (B) Upper: The protocol used to measure the RRP replenishment after a 20 ms depolarisation pulse. Lower: Cm induced by a 20 ms depolarisation applied at various intervals after the conditioning stimulus (n = 8). Data were normalised to the Cm induced by the conditioning pulse, and fit with a bi-exponential function (solid line) where $A_1 = 0.71$, $\tau_1 = 0.26$ s, $A_2 = 0.29$, $\tau_2 = 9.5$ s. (C) Similar to A, except that the conditioning stimulus was 10 pulses of 20 ms depolarisation at 10 Hz. (D) Similar to B, except that the conditioning stimulus was 10 pulses of 20 ms depolarisation at 10 Hz (n = 11). Data were normalised to the Cm induced by a 20 ms depolarisation applied at >30 s after the conditioning stimulus, and fit with a bi-exponential function (solid line) where $A_1 = 0.33$, $\tau_1 = 0.38$ s, $A_2 = 0.67$, $\tau_2 = 7.8$ s. The fitting curve of single pulse was also plotted for comparison (dotted line). (E) Similar to A, except that the conditioning stimulus was 10 pulses of 20 ms depolarisation at 1 Hz. (F) Similar to D, except that the conditioning stimulus was 10 pulses of 20 ms depolarisation at 1 Hz (n = 6). Data were fit with a bi-exponential function where $A_1 = 0.29$, $\tau_1 = 0.25$ s, $A_2 = 0.71$, $\tau_2 = 7.9$ s. (G) The plot of the normalised RRP replenishment_{rapid} amplitude versus calcium influx (QICa) in a 20 ms depolarisation pulse and 10 pulses of 20 ms depolarisation at 1–10 Hz (QICa: 38.9 ± 2.6 pC, n = 8, single pulse; 312 ± 34 pC, n = 11, 10 pulses at 10 Hz; 323 ± 15 pC, n = 6, 10 pulses at 1 Hz).



In the steady state ($t = \infty$), or resting conditions,

$$IP_{\infty} * k_1 = RRP_{\infty} * k_{-1}, \quad (12)$$

$$IP_{\infty} * k_{-2} = RP_{\infty} * k_2. \quad (13)$$

Because the recycling pool, which included RRP_{∞} , IP_{∞} , and RP_{∞} , was 46 times the size of RRP_{∞} ²⁰, where RRP_{∞} , IP_{∞} , and RP_{∞} were all normalised to RRP_{∞} ($RRP_{\infty} = 1$). Thus, $RP_{\infty} = 45 - IP_{\infty}$. These calculations allow us to rewrite equations 12 and 13 as equations 14 and 15:

$$IP_{\infty} * k_1 = 1 * k_{-1}, \quad (14)$$

$$IP_{\infty} * k_{-2} = (45 - IP_{\infty}) * k_2. \quad (15)$$

In equations 8, 9, 14, and 15, t_1 and t_2 (the time constant for rapid and slow RRP replenishment) could be obtained by fitting experimental measurements after a single 20 ms depolarisation with equation 1 (0.26 and 9.5 s, Fig. 1A). The normalised RRP_{∞} was 1, and the normalised $RP_{\infty} = 45 - IP_{\infty}$ ($RRP_{\infty} + IP_{\infty} + RP_{\infty} = 46$). Thus, there are five unknown parameters, k_1 , k_{-1} , k_2 , k_{-2} , and IP_{∞} in four equations (8, 9, 14, 15), which do not allow us to solve these five parameters.

To solve these five parameters, we varied the IP_{∞} value from 0.5 to 10 with an incremental step of 0.1. For each of these IP_{∞} values, we obtained a set of rate constants (k_1 , k_{-1} , k_2 , and k_{-2}) from equations 8, 9, 14, and 15. With each of these IP_{∞} values and their corresponding rate constants (k_1 , k_{-1} , k_2 , and k_{-2}), we numerically calculated the IP, RP, and RRP changes as a function of time after depletion of the RRP by a single 20 ms depolarisation. The numerical calculation was based on equations 3–4 with a Δt of 0.1 ms or less using MATLAB Simbiology toolbox (v2014a, the Mathworks, USA). The calculated RRP replenishment time course was compared to the experimentally measured time course after a 20 ms depolarisation using the Kolmogorov-Smirnov test and the least-squares test. The best fitting group for the parameters is as follows: $IP_{\infty} = 2.7$, $RP = 42.3$, $k_1 = 0.8892$, $k_{-1} = 2.4008$, $k_2 = 0.0093$, and $k_{-2} = 0.1546$ (unit: sec^{-1}).

Results

The rate of the RRP replenishment was slower after more intense stimulation. Many previous studies confirmed that a 10–20 ms depolarisation from -80 to $+10$ mV depletes the RRP at the calyx of Held^{7,26,28,29}. At various times ($\Delta t = 0.05$ – 20 s) after a conditioning 20 ms depolarisation (-80 to $+10$ mV, if not mentioned), which depleted the RRP (459 ± 29 fF, $n = 11$), we applied a 20 ms depolarisation to measure the resulting capacitance jump (ΔC_m), which reflected the recovery of the RRP (Fig. 1A). We also used different intensities of conditioning stimuli, including a single 20 ms depolarisation, and 10 pulses of 20 ms depolarisation delivered at 10 or 1 Hz (Figs. 1C, E). After a 20 ms depolarisation, the RRP recovery could be fitted with a bi-exponential function ($\Delta C_m = A_1 * [1 - \exp(-t/\tau_1)] + A_2 * [1 - \exp(-t/\tau_2)]$) where $A_1 = 0.71$, $\tau_1 = 0.26$ s, $A_2 = 0.29$, $\tau_2 = 9.5$ s (Fig. 1B), which was similar to previous reports^{24–26} (data in Fig. 1 were adopted from our previous study²¹).

After 10 pulses of 20 ms depolarisation at 10 Hz, which induced a capacitance jump of 1260 ± 72 fF ($n = 11$), the RRP replenishment could also fit a bi-exponential function with $A_1 = 0.33$, $\tau_1 = 0.38$ s, $A_2 = 0.67$, $\tau_2 = 7.8$ s (Fig. 1D). Compared to the fitted replenishment curve after a 20 ms depolarisation (dotted curve in Fig. 1D, same as Fig. 1B), the rapid component of replenishment ($\text{replenishment}_{\text{rapid}}$) decreased, whereas the slow component of replenishment ($\text{replenishment}_{\text{slow}}$) increased. Similarly, after 10 pulses of 20 ms depolarisation at 1 Hz, the RRP replenishment also slowed down (Fig. 1F, $A_1 = 0.29$, $\tau_1 = 0.25$ s, $A_2 = 0.71$, $\tau_2 = 7.9$ s). Our results contradict previous studies that suggested a calcium/calmodulin-dependent mechanism^{23,25}. The total calcium charge dramatically increased from a single 20 ms depolarisation pulse to 10 depolarisation pulses of 1 or 10 Hz, but the RRP replenishment slowed down instead of speeding up, which could not be explained by the up-regulation of calmodulin function (Fig. 1G). Furthermore, it is also very interesting that the time constant of the RRP replenishment was very similar among different stimulation protocols (Figs. 1B, D and F).

Rapid and slow vesicle traffic among three pools underlie rapid and slow RRP replenishment. Our observation that the replenishment_{rapid} amplitude was significantly reduced when calcium charge (QICa) was increased by ~ 8 times in Fig. 1G could be resolved if 10 depolarising pulses depleted most of the recycling pool that provided vesicles to the RRP. However, we have shown that the recycling pool was ~ 46 times the size of RRP_{∞} ²⁰, and it was only slightly reduced by 10 depolarising pulses at 1 or 10 Hz, which only released vesicles equivalent to ~ 3 – 6 times the size of RRP. This slight reduction of the recycling pool could not account for the significant decrease in the replenishment_{rapid} amplitude. Therefore, we proposed a new three-pool model to account for this phenomenon (see Methods for details).

From scheme (1), the RRP size can be derived as a function of time after depletion of the RRP. The analytical solution of the RRP (equation 7) is a bi-exponential function, which is consistent with our experimental observation (Figs. 1D, F). Based on the previously measured recycling pool size, which was the sum of the three pools ($RRP_{\infty} + IP_{\infty} + RP_{\infty} = 46$, where ∞ denotes the resting condition and all parameters are normalised to RRP_{∞}), we found that the numerically calculated RRP replenishment time course after a 20 ms depolarisation best fit the observed data (Fig. 1B) when $IP_{\infty} = 2.7$, $RP_{\infty} = 42.3$ (RRP_{∞} was normalised to 1), $k_1 = 0.8892$, $k_{-1} = 2.4008$, $k_2 = 0.0093$, and $k_{-2} = 0.1546 \text{ sec}^{-1}$ (calculated from equations 8–9 and 14–15).

The above parameters were obtained by comparing the model with the observed RRP replenishment after a single 20 ms depolarisation (Fig. 2A, black curve). To further determine whether these parameters were appropriate, we used the model with these parameters to generate several predictions that were not related to the single 20 ms depolarisation data. The prediction was made by numerical calculation of the RRP replenishment using equations 3–4.

First, the model-predicted time course of the RRP replenishment after 10 pulses of 20 ms depolarisation at 10 Hz matched well with the observed time course (Fig. 2B, black curve, $p = 0.93$, K-S test). The predicted time course was fitted by a bi-exponential equation with parameters ($A_1 = 0.37$, $\tau_1 = 0.3$ s, $A_2 = 0.63$, $\tau_2 = 8.3$ s, Fig. 2B, black curve) similar to those obtained from fitting the observed data (Fig. 1D). Second, the model-predicted RRP replenishment matched well with the measured one after 10 depolarising pulses at 1 Hz (Fig. 2C, black curve, $p = 0.90$, K-S test). The model-predicted parameters were also very close to those in observed ones ($A_1 = 0.22$, $\tau_1 = 0.2$ s, $A_2 = 0.78$, $\tau_2 = 6.5$ s). Third, the model-generated exocytosis during each time step matched well with the experimental results. As the model was derived from the RRP replenishment data, it would be supportive if the model could also predict exocytosis. For 10 depolarising pulses at 10 Hz, it is difficult to accurately measure the capacitance jump after each stimulus²⁷, so we only compared the total capacitance jump. The model predicted a total ΔC_m of 2.46 times the RRP evoked by 10 depolarising pulses at 10 Hz. By multiplying this value with the capacitance jump induced by a 20 ms depolarisation, which was the RRP size, it predicted a ΔC_m of 1131 ± 61 fF (1127 ± 61 fF if endocytosed vesicles are not included, $n = 11$), which closely matched the measured ΔC_m after 10 depolarising pulses at 10 Hz (1260 ± 72 fF, $n = 11$, $p = 0.2$, Fig. 2D). For 10 depolarising pulses at 1 Hz, we could accurately compare the capacitance jump after each stimulus. The model predicted a gradual decrease of the capacitance jump induced by each stimulus during 10 depolarising pulses at 1 Hz, which matched the measurement well ($p = 0.7$ with endocytosis, K-S test, Fig. 2E). The predicted total exocytosis amount (with endo: 2.3 ± 0.1 pF, without endo: 2.2 ± 0.1 , $n = 6$) also closely matched the measured net exocytosis (2.3 ± 0.1 pF, $n = 6$, $p = 0.8$ with endocytosis, Fig. 2F). All these matches between predictions and experimental results (Figs. 2B–F) further strengthened our model with parameters described above.

The fast IP-RRP kinetics ($k_1 = 0.8892$, $k_{-1} = 2.4008$) and the slow RP-IP kinetics ($k_2 = 0.0093$, $k_{-2} = 0.1546$) explained why

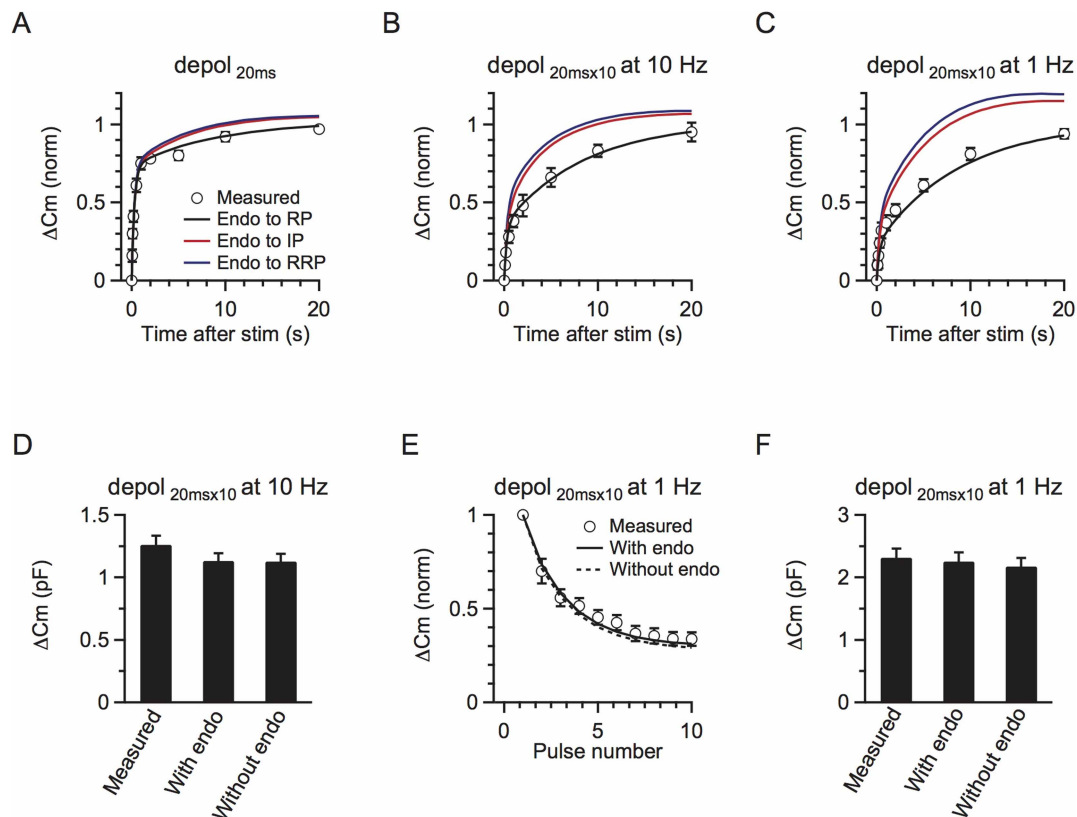


Figure 2 | A three-pool model underlies rapid and slow RRP replenishment. (A) The model-predicted RRP replenishment curves with endocytosed vesicles recycling to RP (black), IP (red) and RRP (blue) after a 20 ms depolarisation pulse. The measured data are also plotted for comparison (circle, same as Fig. 1B). The legend also applies to B and C. (B) Similar to A, but with a conditioning stimulus of 10 pulses of 20 ms depolarisation at 10 Hz. (C) Similar to A and B, but with a conditioning stimulus of 10 pulses of 20 ms depolarisation at 1 Hz. (D) The total measured and predicted ΔC_m with and without endocytosis induced by 10 pulses of 20 ms depolarisation at 10 Hz ($n = 11$). (E) The model-predicted (with endocytosis: black curve, without endocytosis: dotted curve) and the measured (circle) ΔC_m induced by each depolarising pulse (20 ms depolarisation) during a 10-pulse train at 1 Hz. (F) Similar to D, except that the conditioning stimulus was 10 pulses of 20 ms depolarisation at 1 Hz ($n = 6$).

replenishment was bi-exponential with rapid (τ_1) and slow (τ_2) time constants being controlled mostly by k_1 and k_{-1} , and k_2 and k_{-2} , respectively. Our numerical solution to τ_1 and τ_2 also further illustrated why the time constants in different stimulation protocols are roughly the same (equations 8–9). Our numerical calculation (equations 3–4) also showed that the IP size was 2.7 immediately after a 20 ms depolarisation, but decreased to ~ 0.9 – 1.4 immediately after 10 pulses of depolarisation at 1–10 Hz. The IP size after stimulation controlled the replenishment_{rapid} amplitude, which explains why the replenishment_{rapid} component was reduced after 10 pulses of depolarisation at 1–10 Hz.

High temperatures have been shown to lead to accelerated endocytosis³⁰ and faster recovery from synaptic depression at calyces³¹. Recently, ultra-fast endocytosis was observed at hippocampal neurons at 34°C³². To test whether our model could also be applied at physiological temperatures, we performed similar experiments at a more physiological temperature ($\sim 34^\circ\text{C}$). At higher temperatures, RRP replenishment was dramatically accelerated after a 20 ms depolarisation or 10 pulses of 20 ms depolarisation at 1–10 Hz (Figs. S1, see Supplementary Information I for details) and still fit our model well if we multiplied all of the rate constants by a ratio of 2–4.

Neither slow nor rapid endocytosis recycles vesicles within a small recycling pool. We previously showed that both rapid and slow endocytosis do not recycle vesicles within the RRP²¹. The RRP replenishment showed no difference after blocking endocytosis with GTP γ S, which ruled out the possibility of a small recycling pool. We further used the current model to verify this conclusion.

In scheme (1), we compared the influence of endocytosis in three circumstances: 1) endocytosed vesicles directly recycle within the RRP, 2) endocytosed vesicles enter the IP, and 3) the endocytosed vesicles enter the RP. Endocytosed vesicles did not directly enter the RRP because blocking endocytosis did not affect RRP replenishment (Fig. 3). Endocytosed vesicles did not enter the IP because the recycling pool size was 46 times the size of RRP²⁰, whereas the IP _{∞} size was only 2.7. Furthermore, a significant amount of endocytosis occurred during 10 pulses of 20 ms depolarisation at 1 Hz²⁷. If these endocytosed vesicles directly enter the IP, RRP replenishment should be accelerated (Fig. 2C). In contrast, RRP replenishment was slower compared to a single 20 ms depolarisation (Figs. 1D, F). Our model also confirmed that, if the endocytosed vesicles entered the RRP or IP, RRP replenishment would be accelerated, which was not consistent with the experimental observations (Figs. 2A–C). Therefore, we conclude that endocytosed vesicles enter the RP before being mobilised to the IP.

The impact of endocytosis on synaptic transmission. Endocytosis not affecting RRP replenishment raises doubts about the role of endocytosis. To determine the impact of endocytosis during repetitive firing, we mimicked the physiological firing frequency of 50 Hz by depleting the RRP by ~ 6 – 12% for each action potential in our model. We used 50 Hz because the calyx may fire spontaneously at a mean rate of ~ 50 – 60 Hz in vivo³³. We used 6–12% because an action potential may deplete $\sim 6\%$ of the RRP^{34,35} and the release probability may be facilitated by ~ 30 – 100% during stimulation^{36,37}. Based on our previous study²⁷, we assumed that $\sim 70\%$ of fused vesicles were

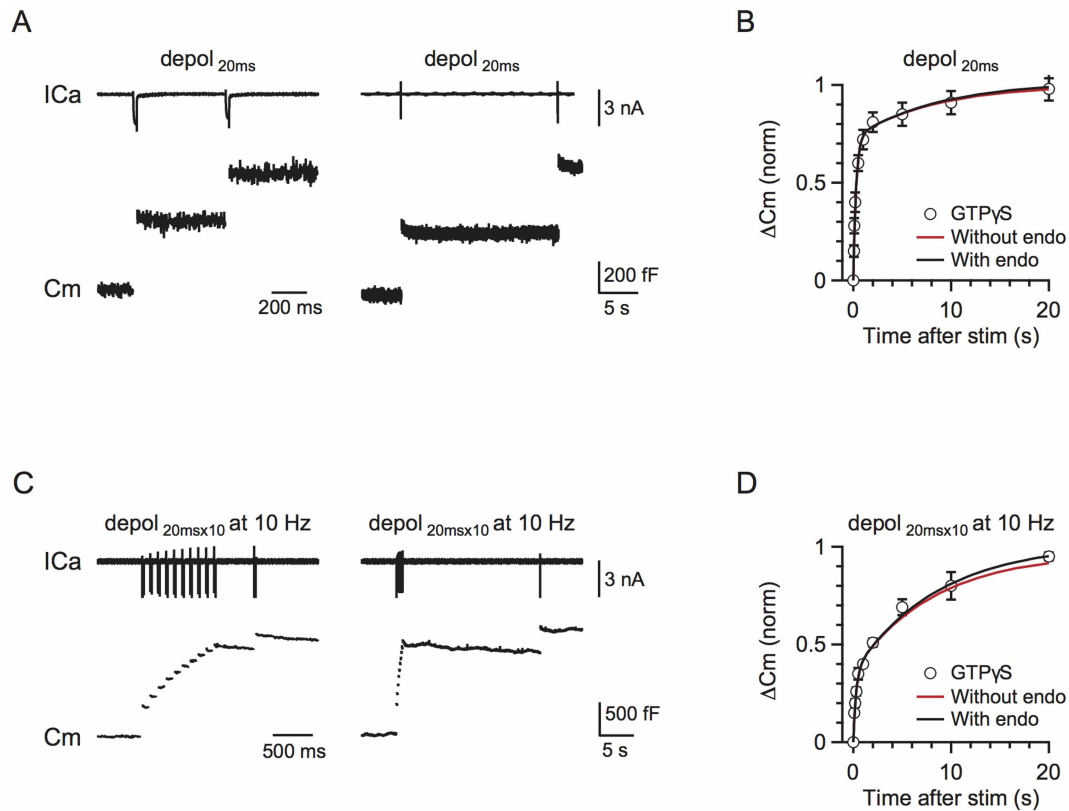


Figure 3 | Rapid and slow endocytosis do not recycle vesicles in a small recycling pool. (A) Left: Sampled presynaptic calcium current (I_{Ca} , upper) and membrane capacitance (C_m , lower) induced by a 20 ms depolarisation applied at 0.5 s after a conditioning pulse of 20 ms depolarization with 0.3 mM GTP γ S in place of GTP in the pipette solution. Right: Similar to Left, except that the stimulus interval is 20 s. (B) The model-predicted RRP replenishment curves with (scheme 1, black) and without endocytosis (scheme 2, red) after a 20 ms depolarisation pulse. Data measured with 0.3 mM GTP γ S in the pipette solution are also plotted for comparison (circle). (C) Similar to A, but with a conditioning stimulus of 10 pulses of 20 ms depolarisation at 10 Hz. (D) Similar to B, except that the conditioning stimulus was 10 pulses of 20 ms depolarisation at 10 Hz.

retrieved rapidly with a time constant of ~ 1.5 s, and the remaining 30% were retrieved slowly with a time constant of ~ 15 s. With scheme (1), the model predicted that the release evoked by a single action potential reached a steady state of 6–11% of the first response (Fig. 4B), which was similar to the steady-state reduction of the EPSCs evoked by axonal fibre stimulation at 50 Hz in the presence of 1 mM kynurenic acid, which prevents postsynaptic AMPA receptor saturation (Figs. 4A–B, $n = 4$ synapses).

In the absence of endocytosis, the model (scheme 2) predicted a gradual decline in release gradually to 0 (Fig. 4C). Compared to the prediction in the presence of endocytosis (scheme 1), the decline was obvious only after stimulation for > 10 s at 50 Hz (Fig. 4C, right). This effect was not trivial to the calyx of Held synapse. The calyx fires spontaneously at a mean rate of ~ 50 Hz in vivo and, without any previous firing, an action potential releases several hundred vesicles that ensure firing of a postsynaptic action potential³³. With firing at 50 Hz, the release induced by an action potential decreases to ~ 6 –11% (Fig. 4B), which is still sufficient to induce a postsynaptic action potential³⁸. Without endocytosis, release will eventually decrease to 0 (Fig. 4C), which abolishes postsynaptic firing. Thus, endocytosis is essential for maintaining transmitter release and synaptic transmission during high frequency firing. We could not confirm this suggestion experimentally by blocking endocytosis with GTP γ S, because a GTP-independent endocytosis develops during strong stimulation³⁹. However, the gradual decrease in release when endocytosis is blocked in *shibire* mutants is consistent with our suggestion^{4,5,40}.

Discussion

Based on our previous finding that both rapid and slow endocytosis recycled vesicles to a large recycling pool instead of within the RRP or

a small recycling pool, we proposed a model composed of three pools, a large RP ~ 42.3 times the size of RRP, a RRP and a small IP ~ 2.7 times the size of RRP in between²⁰. We found that rapid IP-RRP kinetics, slow RP-IP kinetics, and limited IP size are responsible for the rapid and slow components of RRP replenishment, and the slower RRP replenishment with more intense stimulation, as observed at many synapses^{13,22,35,41,42}. This realistic model reveals the contribution of each vesicle cycling step in the maintenance of synaptic transmission, and thus, in the generation and recovery of STD during repetitive stimulation.

There are other explanations for the two components of RRP replenishment. Garcia-Perez et al. reported similar RRP replenishment at hippocampal synapses and provided “delayed depression” as an explanation, which lacked experimental verification⁴³. Otsu et al. proposed two general models that accounted for the fast and slow time constants of RRP replenishment⁴². However, neither model could explain why blocking endocytosis does not affect RRP replenishment. First, our previous results ruled out the possibility that fused vesicles can recycle within the RRP²¹. Second, the relatively small RP size (8–12 times the RRP), which could be dramatically decreased during STD (more than 50% decrease⁴²), and the fast docking/undocking kinetics between RP and RRP suggest a significant role of endocytosis in RRP replenishment, but this is also ruled out by our results. Pyle et al. proposed a similar two-pool model, suggesting that the RRP could be refilled by either rapid retrieval within the RRP or new recruitment from the reserve pool at the hippocampus¹³, which still contradicts our findings²¹. A recent study showed that exocytosed vesicles are not generally reused within 40 s, which further strengthens our conclusion that rapid reuse may not contribute to rapid RRP replenishment⁴⁴. With all parameters experimentally

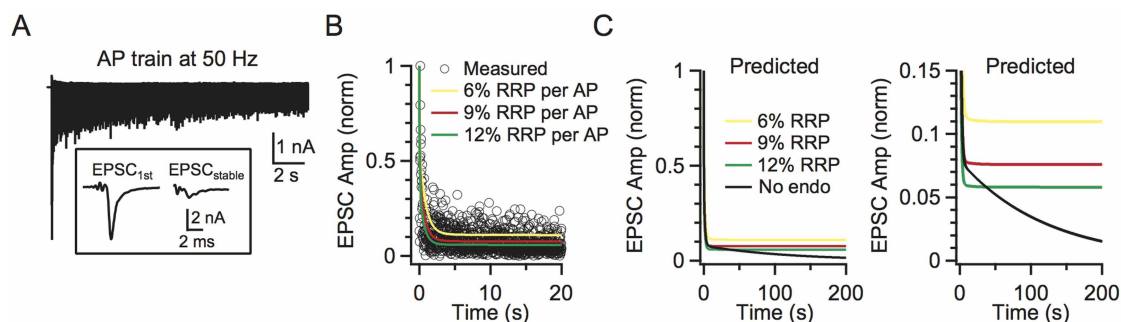


Figure 4 | Impact of endocytosis during high frequency stimulation. (A) Sampled trace of EPSC recordings during a 50 Hz action potential train. Inset shows the large initial EPSC and the small stabilised EPSC for comparison. (B) The model-predicted (curves) and the measured ($n = 4$, circle) amplitudes of the EPSCs during a 50 Hz action potential train. Predicted traces for different depleting percentages after a single action potential are shown in different colours (yellow: 6%, red: 9%, green: 12%). Data were normalised to the first response. Each circle represents the mean amplitude from four synapses (for clarity, s.e.m. is not included). Experimental data were collected from horizontal brain slices, where a bipolar electrode was positioned in the midline of the trapezoid body to induce presynaptic action potentials and thus EPSCs⁵⁴. The model included endocytosis (scheme 1). (C) The model-predicted EPSC amplitude during action potential stimulation at 50 Hz with (scheme 1, colours meanings are the same as B) and without (scheme 2, black) endocytosis. Left and right panels show the same data at different scales.

measured, our model is more quantitatively accurate and more capable of explaining RRP replenishment after different stimulations.

The rapid component of the RRP replenishment time course has been hypothesised to be caused by a calcium/calmodulin-dependent mechanism^{22–25}. A recent study also showed that Munc13-1, the downstream target of the calcium/calmodulin signaling pathway, controls synaptic vesicle replenishment⁴⁵. However, these studies still could not explain our observation of a decrease in the amplitude, but not the time constant, of replenishment_{rapid} with higher calcium influx during more intense stimulation (Figs. 1D, F). Accordingly, our three-pool model solves this problem by adding a small IP, which is responsible for the rapid and slow components of the replenishment time course. The IP controls the amplitude of the replenishment_{rapid}. More intense stimulation caused greater depletion of the IP, which decreased the replenishment_{rapid} amplitude. By ruling out the possibility that rapid RRP replenishment is provided by vesicles made from rapid endocytosis or from a small recycling pool, we conclude that the RRP is replenished from the IP. Although currently more detailed characteristics of this pool remain unclear, a recent study showed that in synapsin triple knock-out mice, the RRP replenishment was significantly slowed down and the number of synaptic vesicles distally from the active zones was strongly decreased, whereas those localised at the active zones remained unchanged⁴⁶. Furthermore, most of the synapsin-defined vesicle pool in that study presented as a part of the traditional RP, comprising ~95% of the total synaptic vesicles^{18,47,48}. Another report using synapsin I/II double knock-out mice proposed a local reserve pool three times the size of RRP at hippocampus⁴⁹, which is also very similar to our conclusion. Morphological evidence from EM also showed that synaptic vesicles could be interconnected by synapsin at a distance from AZ⁵⁰. Our result is consistent with all these findings, and we further include endocytosis to give a more complete vesicle recycling model. It would be of great interest to examine whether synapsin is the key molecular entity that can differentiate the IP from the RP and RRP at calyces in the future¹⁸.

A previous study showing that blocking calmodulin function slowed down endocytosis and RRP replenishment suggested that slowing down of RRP replenishment under stronger stimulation might be caused by occlusion of the active zone by proteins participating in exocytosis^{6,51}. However, a recent report showed that blocking PKA slowed down endocytosis, but did not affect the recruitment of synaptic vesicles to the RRP⁵². Furthermore, under mild stimulation, blocking calmodulin did not block endocytosis but still slowed down RRP replenishment, both of which suggest independent mechanisms

for RRP replenishment and endocytosis⁵². Although our three-pool model was developed for stimulation stronger than a 20 ms depolarisation, it may not necessarily be in conflict with the finding of a calcium/calmodulin-dependent acceleration in the RRP replenishment^{25,53}, as the later mechanism could be saturated by the calcium influx during a single 20 ms depolarisation. Previous studies showed that a 10–20 ms depolarisation pulse can induce enough calcium influx to deplete the RRP at the calyx of Held synapse^{7,26}. In such a case, the slowing of RRP replenishment is dominated by the decrease in IP size. For stimulation milder than a 20 ms depolarisation, our model may be modified to include the calcium effect so that the IP-RRP rate constant (k_1 and k_{-1}) or the IP size is calcium/calmodulin-dependent.

Bi-exponential recovery from STD has been observed in many synapses^{13,22,35,41,42} where our model may also be helpful. For example, at frog auditory hair cell synapses, recovery draws mainly from the preformed vesicles rather than the rapid, freshly endocytosed vesicles, which is consistent with our model⁴⁴. At hippocampal synapses, several new findings, such as the synapsin-mediated vesicle interconnection⁵⁰ and local reserve pool model⁴⁹, also imply the potential usefulness of our model.

Although our three-pool model was proposed from RRP replenishment, it could also be used to accurately dissect the exocytosis at each time step during stimulation (Figs. 2D–F). Furthermore, we evaluated the impact of endocytosis using our three-pool model and concluded that endocytosis is important in maintaining synaptic transmission during high frequency stimulation, which often happens in the central nervous system. Thus, we concluded that the three-pool model is a useful tool for revealing the contribution of each vesicle cycling step in the maintenance of synaptic transmission, and the generation and recovery of STD during repetitive stimulation.

1. Regehr, W. G. Short-term presynaptic plasticity. *Cold Spring Harbor perspectives in biology* **4**, a005702, doi:10.1101/cshperspect.a005702 (2012).
2. Abbott, L. F. & Regehr, W. G. Synaptic computation. *Nature* **431**, 796–803 (2004).
3. Betz, W. J. Depression of transmitter release at the neuromuscular junction of the frog. *J. Physiol.* **206**, 629–644 (1970).
4. Koenig, J. H. & Ikeda, K. Synaptic vesicles have two distinct recycling pathways. *J. Cell Biol.* **135**, 797–808 (1996).
5. Delgado, R., Maureira, C., Oliva, C., Kidokoro, Y. & Labarca, P. Size of vesicle pools, rates of mobilization, and recycling at neuromuscular synapses of a *Drosophila* mutant, shibire. *Neuron* **28**, 941–953 (2000).
6. Wu, X. S. *et al.* Ca(2+) and calmodulin initiate all forms of endocytosis during depolarization at a nerve terminal. *Nat. Neurosci.* **12**, 1003–1010, doi:10.1038/nn.2355 (2009).



7. Xue, L. *et al.* Voltage-dependent calcium channels at the plasma membrane, but not vesicular channels, couple exocytosis to endocytosis. *Cell Rep.* **1**, 632–638, doi:10.1016/j.celrep.2012.04.011 (2012).
8. He, L. & Wu, L. G. The debate on the kiss-and-run fusion at synapses. *Trends Neurosci.* **30**, 447–455 (2007).
9. Albillos, A. *et al.* The exocytotic event in chromaffin cells revealed by patch amperometry. *Nature* **389**, 509–512 (1997).
10. Klyachko, V. A. & Jackson, M. B. Capacitance steps and fusion pores of small and large-dense-core vesicles in nerve terminals. *Nature* **418**, 89–92 (2002).
11. Aravanis, A. M., Pyle, J. L. & Tsien, R. W. Single synaptic vesicles fusing transiently and successively without loss of identity. *Nature* **423**, 643–647 (2003).
12. He, L., Wu, X. S., Mohan, R. & Wu, L. G. Two modes of fusion pore opening revealed by cell-attached recordings at a synapse. *Nature* **444**, 102–105 (2006).
13. Pyle, J. L., Kavalali, E. T., Piedras-Renteria, E. S. & Tsien, R. W. Rapid reuse of readily releasable pool vesicles at hippocampal synapses. *Neuron* **28**, 221–231 (2000).
14. Harata, N. C., Aravanis, A. M. & Tsien, R. W. Kiss-and-run and full-collapse fusion as modes of exo-endocytosis in neurosecretion. *J. Neurochem.* **97**, 1546–1570 (2006).
15. Ertunc, M. *et al.* Fast synaptic vesicle reuse slows the rate of synaptic depression in the CA1 region of hippocampus. *J Neurosci* **27**, 341–354 (2007).
16. Jockusch, W. J., Praefcke, G. J., McMahon, H. T. & Lagnado, L. Clathrin-dependent and clathrin-independent retrieval of synaptic vesicles in retinal bipolar cells. *Neuron* **46**, 869–878 (2005).
17. Granseth, B., Odermatt, B., Royle, S. J. & Lagnado, L. Clathrin-mediated endocytosis is the dominant mechanism of vesicle retrieval at hippocampal synapses. *Neuron* **51**, 773–786 (2006).
18. Rizzoli, S. O. & Betz, W. J. Synaptic vesicle pools. *Nat. Rev. Neurosci.* **6**, 57–69 (2005).
19. Sätzler, K. *et al.* Three-dimensional reconstruction of a calyx of Held and its postsynaptic principal neuron in the medial nucleus of the trapezoid body. *J Neurosci* **22**, 10567–10579 (2002).
20. Xue, L. *et al.* Most vesicles in a central nerve terminal participate in recycling. *J Neurosci* **33**, 8820–8826, doi:10.1523/JNEUROSCI.4029-12.2013 (2013).
21. Wu, X. S. & Wu, L. G. Rapid endocytosis does not recycle vesicles within the readily releasable pool. *J Neurosci* **29**, 11038–11042, doi:10.1523/JNEUROSCI.2367-09.2009 (2009).
22. Dittman, J. S. & Regehr, W. G. Calcium dependence and recovery kinetics of presynaptic depression at the climbing fiber to Purkinje cell synapse. *J Neurosci* **18**, 6147–6162 (1998).
23. Wang, L.-Y. & Kaczmarek, L. K. High-frequency firing helps replenish the readily releasable pool of synaptic vesicles. *Nature* **394**, 384–388 (1998).
24. Wu, L. G. & Borst, J. G. G. The reduced release probability of releasable vesicles during recovery from short-term synaptic depression. *Neuron* **23**, 821–832 (1999).
25. Sakaba, T. & Neher, E. Calmodulin mediates rapid recruitment of fast-releasing synaptic vesicles at a calyx-type synapse. *Neuron* **32**, 1119–1131 (2001).
26. Sun, J. Y. & Wu, L. G. Fast kinetics of exocytosis revealed by simultaneous measurements of presynaptic capacitance and postsynaptic currents at a central synapse. *Neuron* **30**, 171–182 (2001).
27. Wu, W., Xu, J., Wu, X. S. & Wu, L. G. Activity-dependent acceleration of endocytosis at a central synapse. *J Neurosci* **25**, 11676–11683 (2005).
28. Taschenberger, H., Leao, R. M., Rowland, K. C., Spirou, G. A. & Von Gersdorff, H. Optimizing synaptic architecture and efficiency for high-frequency transmission. *Neuron* **36**, 1127–1143 (2002).
29. Sun, J. *et al.* A dual-Ca²⁺-sensor model for neurotransmitter release in a central synapse. *Nature* **450**, 676–682 (2007).
30. Renden, R. & von Gersdorff, H. Synaptic vesicle endocytosis at a CNS nerve terminal: faster kinetics at physiological temperatures and increased endocytotic capacity during maturation. *J Neurophysiol* **98**, 3349–3359, doi:10.1152/jn.00898.2007 (2007).
31. Kushmerick, C., Renden, R. & von Gersdorff, H. Physiological temperatures reduce the rate of vesicle pool depletion and short-term depression via an acceleration of vesicle recruitment. *J Neurosci* **26**, 1366–1377, doi:10.1523/jneurosci.3889-05.2006 (2006).
32. Watanabe, S. *et al.* Ultrafast endocytosis at *Caenorhabditis elegans* neuromuscular junctions. *eLife* **2**, e00723, doi:10.7554/eLife.00723 (2013).
33. von, G. H. & Borst, J. G. Short-term plasticity at the calyx of Held. *Nat. Rev. Neurosci.* **3**, 53–64 (2002).
34. Schneggenburger, R., Sakaba, T. & Neher, E. Vesicle pools and short-term synaptic depression: lessons from a large synapse. *Trends Neurosci.* **25**, 206–212 (2002).
35. Xu, J. & Wu, L. G. The decrease in the presynaptic calcium current is a major cause of short-term depression at a calyx-type synapse. *Neuron* **46**, 633–645 (2005).
36. Felmy, F., Neher, E. & Schneggenburger, R. Probing the intracellular calcium sensitivity of transmitter release during synaptic facilitation. *Neuron* **37**, 801–811 (2003).
37. Xu, J., He, L. & Wu, L. G. Role of Ca(2+) channels in short-term synaptic plasticity. *Curr. Opin. Neurobiol.* **17**, 352–359 (2007).
38. Wu, L. G. & Betz, W. J. Kinetics of synaptic depression and vesicle recycling after tetanic stimulation of frog motor nerve terminals. *Biophys. J.* **74**, 3003–3009 (1998).
39. Xu, J. *et al.* GTP-independent rapid and slow endocytosis at a central synapse. *Nat. Neurosci.* **11**, 45–53 (2008).
40. Koenig, J. H. & Ikeda, K. Disappearance and reformation of synaptic vesicle membrane upon transmitter release observed under reversible blockage of membrane retrieval. *J Neurosci* **9**, 3844–3860 (1989).
41. Cho, S., Li, G. L. & von Gersdorff, H. Recovery from short-term depression and facilitation is ultrafast and Ca²⁺ dependent at auditory hair cell synapses. *J Neurosci* **31**, 5682–5692, doi:10.1523/jneurosci.5453-10.2011 (2011).
42. Otsu, Y. *et al.* Competition between phasic and asynchronous release for recovered synaptic vesicles at developing hippocampal autaptic synapses. *J Neurosci* **24**, 420–433, doi:10.1523/JNEUROSCI.4452-03.2004 (2004).
43. Garcia-Perez, E., Lo, D. C. & Wesseling, J. F. Kinetic isolation of a slowly recovering component of short-term depression during exhaustive use at excitatory hippocampal synapses. *J Neurophysiol* **100**, 781–795, doi:10.1152/jn.90429.2008 (2008).
44. Hua, Y. *et al.* Blocking endocytosis enhances short-term synaptic depression under conditions of normal availability of vesicles. *Neuron* **80**, 343–349, doi:10.1016/j.neuron.2013.08.010 (2013).
45. Lipstein, N. *et al.* Dynamic Control of Synaptic Vesicle Replenishment and Short-Term Plasticity by Ca²⁺-Calmodulin-Munc13-1 Signaling. *Neuron* **79**, 82–96, doi:10.1016/j.neuron.2013.05.011 (2013).
46. Vasileva, M., Horstmann, H., Geumann, C., Gitler, D. & Kuner, T. Synapsin-dependent reserve pool of synaptic vesicles supports replenishment of the readily releasable pool under intense synaptic transmission. *The European journal of neuroscience* **36**, 3005–3020, doi:10.1111/j.1460-9568.2012.08255.x (2012).
47. Denker, A. & Rizzoli, S. O. Synaptic vesicle pools: an update. *Frontiers in synaptic neuroscience* **2**, 135, doi:10.3389/fnsyn.2010.00135 (2010).
48. Orenbuch, A. *et al.* Synapsin selectively controls the mobility of resting pool vesicles at hippocampal terminals. *J Neurosci* **32**, 3969–3980, doi:10.1523/JNEUROSCI.5058-11.2012 (2012).
49. Gabriel, T. *et al.* A new kinetic framework for synaptic vesicle trafficking tested in synapsin knock-outs. *J Neurosci* **31**, 11563–11577, doi:10.1523/JNEUROSCI.1447-11.2011 (2011).
50. Siksou, L. *et al.* Three-dimensional architecture of presynaptic terminal cytomatrix. *J Neurosci* **27**, 6868–6877, doi:10.1523/JNEUROSCI.1773-07.2007 (2007).
51. Wu, L. G., Hamid, E., Shin, W. & Chiang, H. C. Exocytosis and endocytosis: modes, functions, and coupling mechanisms. *Annu Rev Physiol* **76**, 301–331, doi:10.1146/annurev-physiol-021113-170305 (2014).
52. Yao, L. & Sakaba, T. Activity-dependent modulation of endocytosis by calmodulin at a large central synapse. *Proc Natl Acad Sci U S A* **109**, 291–296, doi:10.1073/pnas.1100608109 (2012).
53. Hosoi, N., Sakaba, T. & Neher, E. Quantitative analysis of calcium-dependent vesicle recruitment and its functional role at the calyx of Held synapse. *J Neurosci* **27**, 14286–14298 (2007).
54. Borst, J. G. G., Helmchen, F. & Sakmann, B. Pre- and postsynaptic whole-cell recordings in the medial nucleus of the trapezoid body of the rat. *J. Physiol.* **489**, 825–840 (1995).

Acknowledgments

This work was sponsored by Shanghai Pujiang Program, National Natural Science Foundation of China (grant number: 31370828), Specialised Research Fund for the Doctoral Program of Higher Education (SRFDPF, grant number: 20120071120013) and the Shanghai Leading Academic Discipline Project (B111).

Author contributions

J.G. and L.X. designed research; J.-L.G., M.H. and X.-S.W. performed experiments; J.G., Z.-C.S. and L.X. built the model; J.-B. Z., W.W. and P.-T.Y. helped with experiments; W.L. helped verify the model and L.X. supervised the project and wrote the paper.

Additional information

Supplementary information accompanies this paper at <http://www.nature.com/scientificreports>

Competing financial interests: The authors declare no competing financial interests.

How to cite this article: Guo, J. *et al.* A Three-Pool Model Dissecting Readily Releasable Pool Replenishment at the Calyx of Held. *Sci. Rep.* **5**, 9517; DOI:10.1038/srep09517 (2015).



This work is licensed under a Creative Commons Attribution 4.0 International License. The images or other third party material in this article are included in the article's Creative Commons license, unless indicated otherwise in the credit line; if the material is not included under the Creative Commons license, users will need to obtain permission from the license holder in order to reproduce the material. To view a copy of this license, visit <http://creativecommons.org/licenses/by/4.0/>